HERCULES-2 Project

Fuel Flexible, Near Zero Emissions, Adaptive Performance Marine Engine

Deliverable: D2.6

Development and application of optical techniques for multi-fuel studies

Revision Final

Nature of the Deliverable:	Report
Due date of the Deliverable:	01.05.2018
Actual Submission Date:	14.05.2018
Dissemination Level:	Public

Contributors:	18 - LUND
	19 - MDT

Work Package Leader Responsible: Johan Hult, (MDT)

Start date of Project: 01/05/2015 Duration: 42 months

Grant Agreement No: **634135-HERCULES-2**

HORIZON 2020

The EU Framework Programme for Research and Innovation

TABLE OF CONTENTS

Executive Summary 3
1 Introduction 5
2 Objectives 6
3 Development and Application Work 6
3.1 In-cylinder High-Speed Imaging of Ethane combustion 6
3.2 3D Flame Imaging of Diesel and Natural Gas Flames 7
3.2.1 Motivation 7
3.2.2 Experimental arrangement and calibration 8
3.2.3 Space Carving 9
3.2.4 Diesel operation 10
3.2.5 Natural gas operation 12
3.3 Schlieren Imaging 14
3.3.1 Introduction 14
3.3.2 Experimental results with Schlieren techniques 17
3.4 Lubrication Oil Visualization 21
3.4.1 Introduction 21
3.4.2 Experimental Setup 21
3.4.3 Identifying suitable tracer species 23
3.4.4 Results 26
4 References 32

Executive Summary

High-Speed and 3D imaging of the combustion process

Initially, Ethane combustion was studied with high-speed imaging techniques. Then a calibrated multiple high-speed camera arrangement recording the flame emission from three different directions was used for studying both diesel and natural gas flames on the MDT 4T50ME-X test engine. From the multiple views the flame position inside the engine cylinder can be spatially mapped, allowing quantitative studies of the dynamics of ignition, flame development and propagation for operation on both fuels. Through space carving the three-dimensional (3D) flame contour can be estimated. From this contour properties like flame length, flame height, ignition locations and flame directions can be extracted.

The flame was viewed simultaneously using three high-speed cameras. Optical access was achieved using borescopes, inserted into optical inserts with a sapphire window at the tip which extends into the combustion chamber. The inserts were mounted in ports otherwise used for fuel injectors at the top of the cylinder cover. As the inserts were tilted 15° and the borescope direction of view was 70° a side view into the combustion chamber was obtained. Two of the cameras were of the model Photron SA-Z and one camera of the model Photron SA-X2. Three cameras were used to image the flame luminosity from three different directions, in order to allow a spatial localization of the flame inside the engine cylinder. By using high-speed cameras, operated at a constant frame rate of 10000 frames per second, this allows the dynamics and variations in flame propagation to be followed in individual engine cycles.

The camera views and the effective camera positions, which are given by the borescope tip lens positions, were determined using a calibration method. This part of part of the calibration was implemented in Matlab, relying on imaging of a reference chess-board target positioned at various locations inside the combustion chamber. For 3D-visualisation of the flame location, a space carving method was used. The flame contours from the three separate cameras acted as input. Initially, the entire cylinder interior is filled with voxels representing potential flame locations. For each camera, all the voxels falling outside the observed flame contours, are then carved away. The voxels that remain after carving, correspond to a possible flame location based on the three views recorded. The space carved volume overestimates the flame volume, as it is the convex hull that is left after carving. Certain features are, however, reasonably well captured by the carving. The first is the location and time of the first ignition point. The second is the flame tip, which is the furthest distance from the fuel injector to the front of the flame and which thus gives an estimate of the flame length. The third is the height of the flame, as both the highest and lowest points on the flame are captured well by the carving. The extent of the flame towards the centre of the cylinder is also quite well captured. Tomographic reconstruction has also been investigated but with the limited field of views available, the space carving approach proved to be superior.

Development of High-Speed Schlieren and laser speckle imaging

Normally, density variations are invisible to the human eye, until a background pattern is placed behind them, or light traverses through them and the refraction can be observed. The Schlieren technique, along with the Shadowgraph technique, is an optical method that can visualize and evaluate density variations in fluids. This imaging technique is also applicable in flames and evaporating sprays and it is possible to derive parameters such as temperature, accurate liquid and gaseous penetration lengths. Combined with high speed imaging, it becomes a powerful tool that can temporally resolve highly transient phenomena such as those found in high-pressure fuel injection.

A modular Z-type Schlieren setup was developed for the purposes of this project. A 2 Watt, 452nm laser diode was used as the light source, since it can be found at very low cost and produces high power, coherent and narrowband light. The laser diode was coupled to a 600μm optical fiber in order to provide a physically small light source that provides a circular diverging beam, thus providing an ideal light source for a Schlieren application. Other configurations were tested as well, with diffuser lenses in front of the laser diode that essentially reduce the coherence and scatter light, leading to an extended source and a more uniform background, thus increasing the dynamic range of the setup. Two 75mm diameter parabolic mirrors with a focal distance of 500mm were used in order to collimate and refocus the laser light. Mirrors are preferred over lenses, since they don't introduce aberrations and they are readily available in big sizes. A Photron SA-5 high speed camera was used to obtain the Schlieren images since the purpose was to characterize the injection and combustion inside the 4T50ME-X test engine with the optical cover fitted that allows for a view straight through the combustion chamber. All the components were mounted on two flat aluminum beams with sliding carriers for quick and secure positioning. Thus the whole setup can be moved to the measurement location, pre-aligned, with only minor adjustments necessary on-site.

In addition to the above mentioned Schlieren imaging, the concept of Laser speckle-Background Oriented Schlieren (BOS) was investigated. The laser power was kept low which provided a more pronounced speckle pattern. In principle, this optical setup is used to create Shadowgraph images. However, the detection of the density gradients is not based on the contrast or the brightness of the image regions anymore. Instead, the motion, or the changes in the speckle pattern are evaluated over a background image that doesn't have any disturbances. The rays that create the speckle pattern will be the same, however, they will be deflected to a different position due to density gradients. When comparing to the background image, the displacement of the speckles can be evaluated by direct cross correlation. After use of a high-pass filter, the recorded image looks almost identical to a typical PIV image and can thus be analyzed in a manner similar to PIV images. In other words, with a single frame and a reference image the density gradients can be characterized in both magnitude and direction. This BOS technique constitutes a simpler and more robust approach compared to traditional Schlieren imaging.

In-cylinder visualization of lubricant oil distribution

Engine lubrication is very important for engine sustainability and efficiency. It becomes even more important when heavier fuel types who contributes to lubrication are changed to alternative fuel without the same lubrication abilities. In such situations, one wants to be sure that the lubricant oil reaches all the important locations in the engine.

The in-cylinder visualization of lubricant oil can be studied using a variation of LIF (Laser induced fluorescence) technique that revolves around shining laser light inside the engine to receive back an emission signal from an excited fluorescence dye that has been applied to the lubrication oil. This received signal will then tell us about the current distribution of the lubricant oil. Furthermore, the use of LIF has some benefits as a detection technique, such as the ability to measure non-intrusively while the engine is running, enabling a realistic measurement environment. A reason for applying the fluorescence dye to only new oil coming into the system from the oil pump, is to be able to monitor its dispersion and mixing with the oil already present inside the engine.

This part of the diagnostics work aims at identifying a suitable fluorescence dye for use in LIF experiments to trace lubricant oil inside marine engines. To be considered suitable as oil tracer, the fluorescence dye must have a strong quantum yield, be compatible with temperatures normal for a marine engine and perturb the lubricant oils characteristics as little as possible.

Several potential dye candidates have been selected for investigation, based on previous research in the similar fields. These dyes are then evaluated in a laboratory environment using a frequency doubled (532 nm) Nd-YAG laser. The choice of using a wavelength of 532 nm was made to reduce the amount of fluorescence from the oil itself as the oil will fluorescence much more if shorter wavelengths would be employed. The tracer species were studied with focus on solubility, intensities and temperature resistivity.

During the measurement, the oil sample was kept inside an Erlenmeyer flask made of glass, this flask type is highly thermal resistant and possess low absorption of maximum 10 percent in the spectral range of interest. The heating of the sample was performed by a heating plate, able to increase the temperature of the sample to 150°C. The temperature range was chosen to cover the normal marine engine liner temperatures of 75-125°C.

Among the investigated candidates, Pyrromethene 650 was chosen as the most suitable tracer for the lubricant oil, due to the dyes spectral red shift giving the ability to filter away the fluorescence spectrum of the lubricant oil itself. This makes easy to distinguish the traced lubricant oil from the non-traced oil. The lab result from visualizing Pyrromethene 650 traced lubricant oil by 2D imaging with an ICCD camera, show that it is feasible to generate images with good signal to noise ratio already with moderate laser energies. In total, the outcome of this study is highly promising for the upcoming in-cylinder applications.

1 Introduction

This Work Package is focused on the development and application of non-intrusive optical measurement techniques for studies on marine engines operating on alternative fuels. One clear

technology gap that has been addressed is the lack of 3D information on the early flame development. Also the 3D flame topology, position and overall size are very hard to probe experimentally. Such knowledge is important to have, especially for model validation purposes. The ability to temporally resolve the processes in one single engine cycle is also of major interest. For this reason the majority of the work has been performed in the domain referred to as high-speed diagnostics. To address the need for 3D flame data, both tomographic and space carving approaches have been investigated. For spray characterization, Schlieren and Schlieren-related techniques have been utilized. Another area of interest when operating on alternative fuels is the lubrication system. Here a technique for tracking the in-cylinder distribution of lubricant oil has been developed and a suitable tracer species has been identified.
The first topic (3D imaging) has been applied to the two-stroke test engine at MDT, whereas the last two (Schlieren and lubrication) are scheduled be applied to the engine during the project extension period.

2 Objectives

The main objectives have been to develop and apply diagnostics techniques for in-cylinder investigations in marine engines running on alternative fuels. To address the industry needs several different topics have been investigated. Key parameters when adopting an alternative fuel are, among others, the liquid and gaseous fuel penetration during the injection event, ignition and early flame development, flame topology in 3 dimensions, etc. Also the performance of the lubrication system becomes highly important when running on fuel with poor lubrication capabilities. These aspects have all been in the focus of this Work-Package.

3 Development and Application Work

3.1 In-cylinder High-Speed Imaging of Ethane combustion

Optical high-speed imaging has been used to study combined ethane and diesel fuel combustion on the test engine in Copenhagen, see Fig. 1. Two cameras and borescopes were mounted on the test engine in Copenhagen, which was operated with ethane in the gas supply and with diesel pilots for ignition. The cameras were operated at 20000 frames per second frame rate. The ethane flame, see Fig. 2, was impossible to distinguish from the diesel flame visually, which is in contrast to previous experiments on natural gas which produces a less bright flame than the diesel (see data in next section). From the right view the spatial extent of the flames is visually similar in the two running modes. From the left view (more of a front view), however, the ethane flame is seen to bulge out to the upper left part of the image. This indicates that it is crucial to pick the right observation direction if one is to study differences in flame topology when multiple fuel injectors are used, such as on a multi-fuel engine as this one.

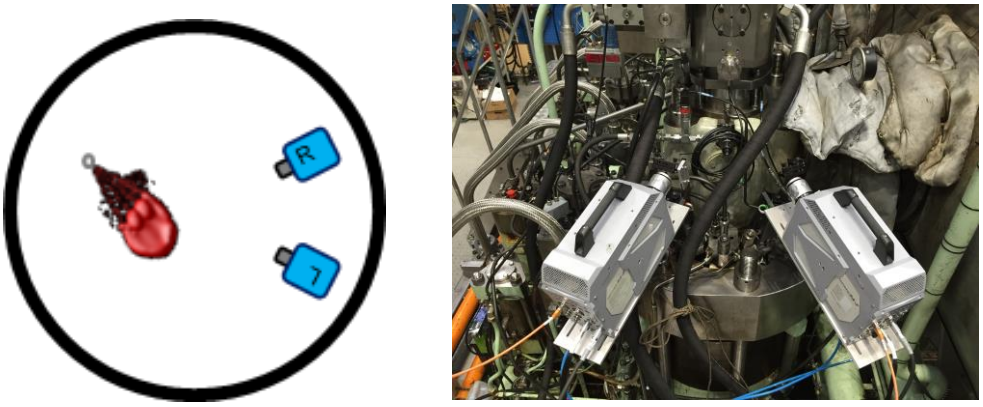

Fig. 1. Set-up for dual camera flame imaging of ethane combustion on T50ME-X test engine.

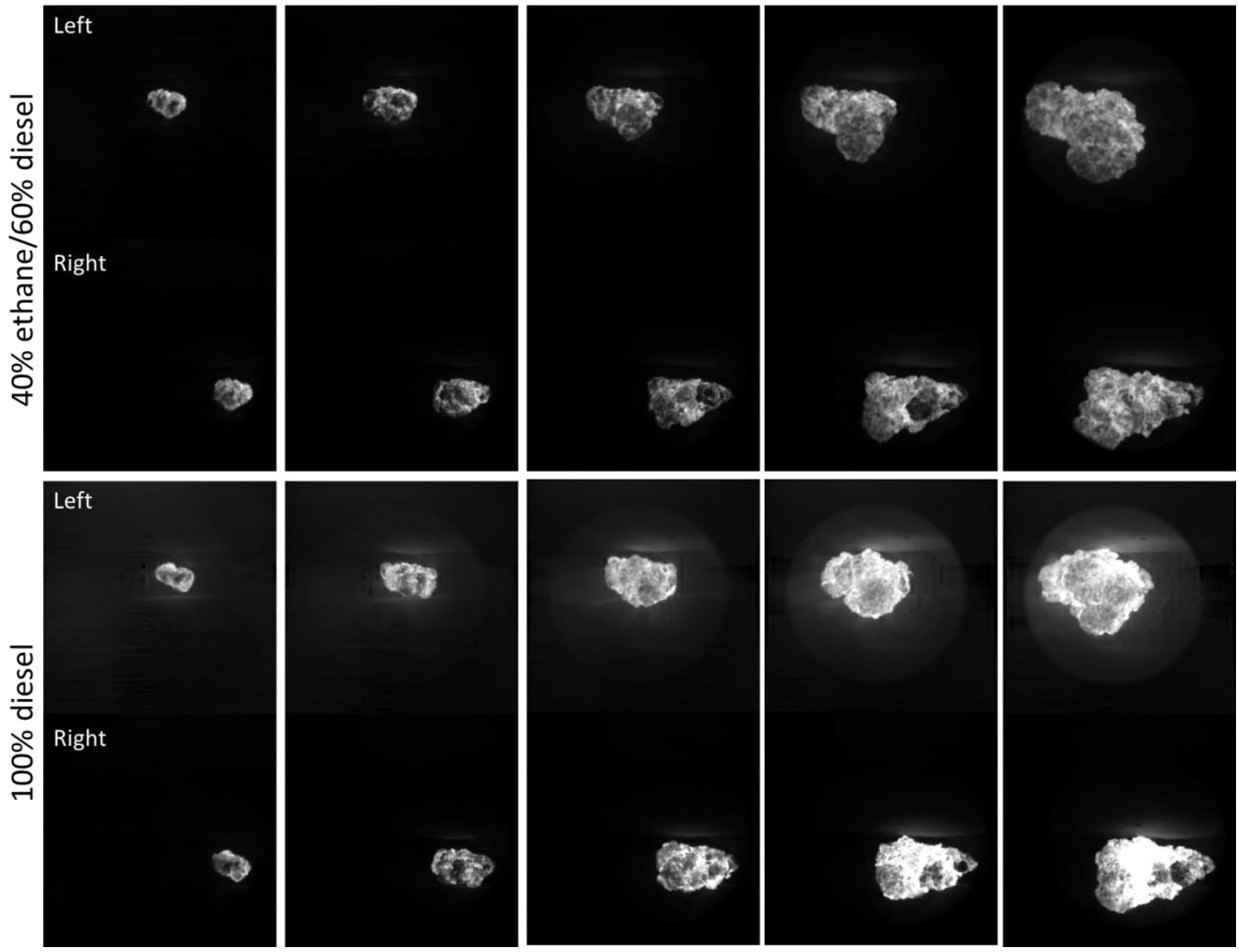

Fig. 2. Mixed mode ethane/diesel flame and pure diesel flame viewed from the left (L) and right (R) high-speed cameras.

3.2 3D Flame Imaging of Diesel and Natural Gas Flames

3.2.1 Motivation

A calibrated multiple high-speed camera arrangement recording the flame emission from three different directions was used for studying both diesel and natural gas flames on the MDT 4T50ME-X test engine. From the multiple views the flame position inside the engine cylinder can be spatially mapped, allowing quantitative studies of the dynamics of ignition, flame development and propagation for operation on both fuels. Through space carving the three-dimensional (3D) flame

contour can be estimated. From this contour properties like flame length, flame height, ignition locations and flame directions can be extracted.

3.2.2 Experimental arrangement and calibration

The engine used for the optical experiments was the MAN Diesel&Turbo 4T50ME-X test engine. It is a production sized turbocharged low-speed two-stroke Diesel engine. It has four cylinders with a bore of 0.5 m and a stroke of 2.2 m. The engine is of the uniflow scavenged type, with air intake ports at the bottom of the cylinder and a centrally located exhaust valve at the top. The in-cylinder flow is defined by a strong swirling motion introduced with the scavenging air. In standard configuration each cylinder is equipped with two diesel fuel injectors and two natural gas injectors placed around the rim of the cylinder and injecting tangentially along the swirl direction.

The flame was viewed simultaneously using three high-speed cameras, see Fig. 3. Optical access was achieved using borescopes, inserted into optical inserts with a sapphire window at the tip which extends into the combustion chamber. The inserts were mounted in ports otherwise used for fuel injectors at the top of the cylinder cover [1]. As the inserts were tilted 15° and the borescope direction of view was 70° a side view into the combustion chamber was obtained. Two of the cameras (1&2) were of the model Photron SA-Z and one (camera 3) of the model Photron SA-X2. Here all cameras were operated at a constant frame rate of 10000 frames per second and with an exposure time of 6.25 μs.

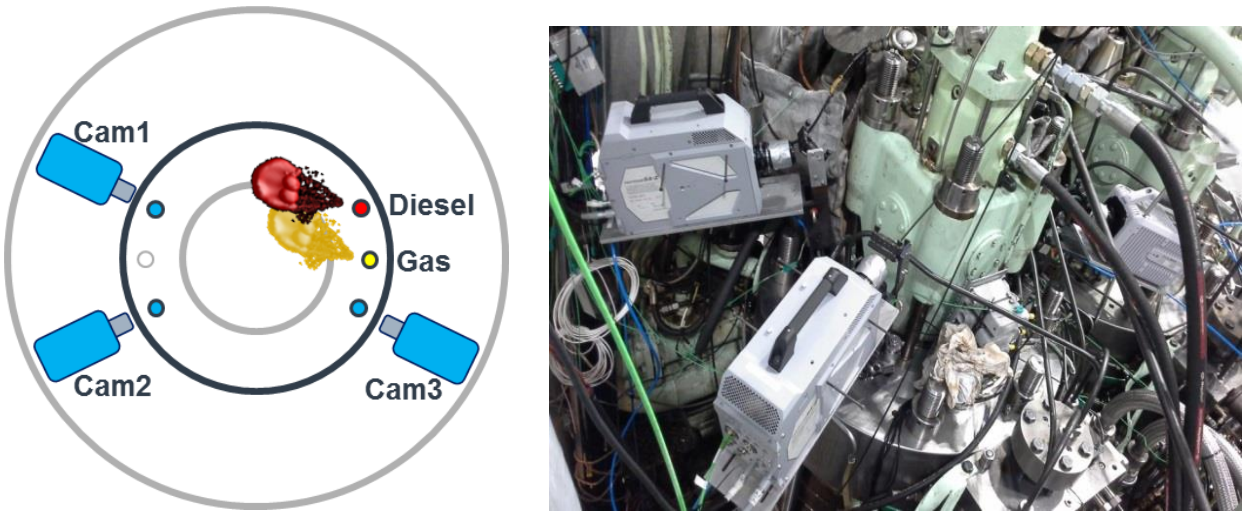

Fig. 3. Set-up for tri-camera flame imaging on T50ME-X test engine.

Three high-speed cameras were used to image the flame luminosity from three different directions, in order to allow a spatial localisation of the flame inside the engine cylinder. By using high-speed cameras this allows the dynamics and variations in flame propagation to be followed in individual engine cycles. In order to allow an unobstructed optical view of the flame the test cylinder was operated with only a single diesel fuel injector and a single gas injector, as illustrated in Fig 3. Camera 1 then provided a view of the flame from the front, camera 2 from the side and camera 3 slightly from behind. The camera views and the effective camera positions (actually given by the borescope tip lens positions) were determined using a calibration method

(implemented in Matlab) relying on imaging a chess-board target positioned at various locations inside the combustion chamber [2]. In Fig. 4 an example of three views of the same calibration target are shown, with the identified calibration points and the reprojected points, calculated from the calibration.

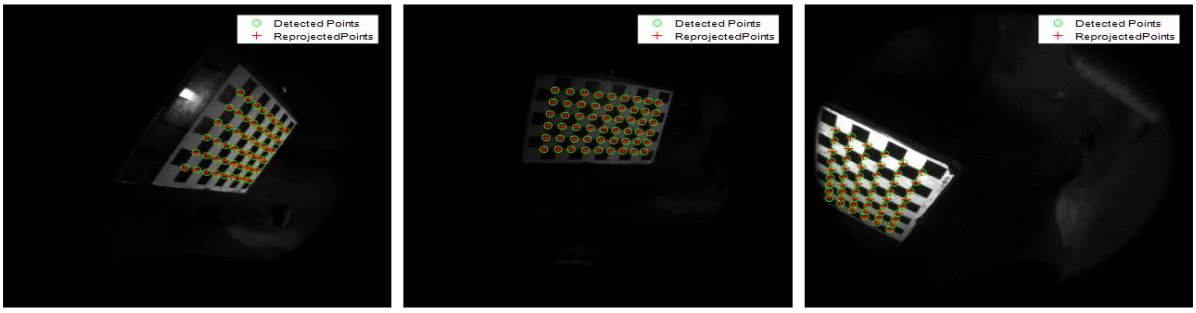

Fig. 4. Example of chess-board target used for calibrating the camera set-up as viewed from the three cameras. Detected calibrations points marked with green circles and reprojected points marked with red crosses.

The calculated camera positions relative to the calibration target positions are shown in 3D in Fig. 5.

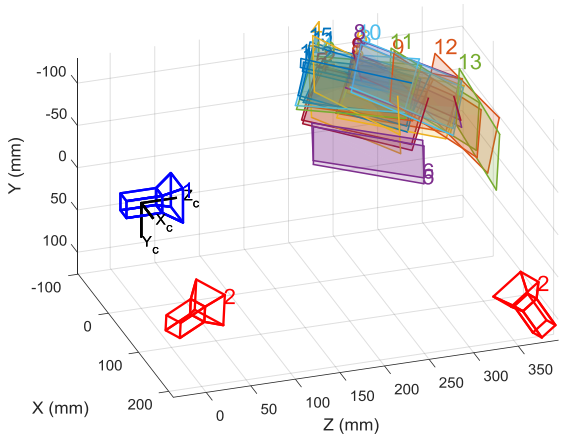

Fig. 5. Result of camera calibrations, with camera and calibration target positions plotted.

3.2.3 Space Carving

For visualisation of the flame location a space carving method was used, with the segmented flame contours from the three cameras as input [3]. Three example flame contours are shown in the top row of Fig. 6. To start with the entire cylinder interior is filled with voxels representing potential flame locations (bottom row, left). For each camera one then carves away all the voxels falling outside the observed flame contours (bottom row, middle). In the bottom row (right) the voxels remaining after the carving are shown. Those voxels correspond to a possible flame location based on the three views recorded. The thus space carved volume overestimates the flame volume, as it is the convex hull that is left after carving. Certain features are, however, still reasonably well captured by the carving. The first is the location and time of the first ignition point. The second is the flame tip, which is the furthest distance from the fuel injector to the front of the flame and which thus gives an estimate of the flame length. The third is the height of the flame, as

both the highest and lowest points on the flame are captured well by the carving. The extent of the flame towards the centre of the cylinder (towards camera 2) is also quite well captured.

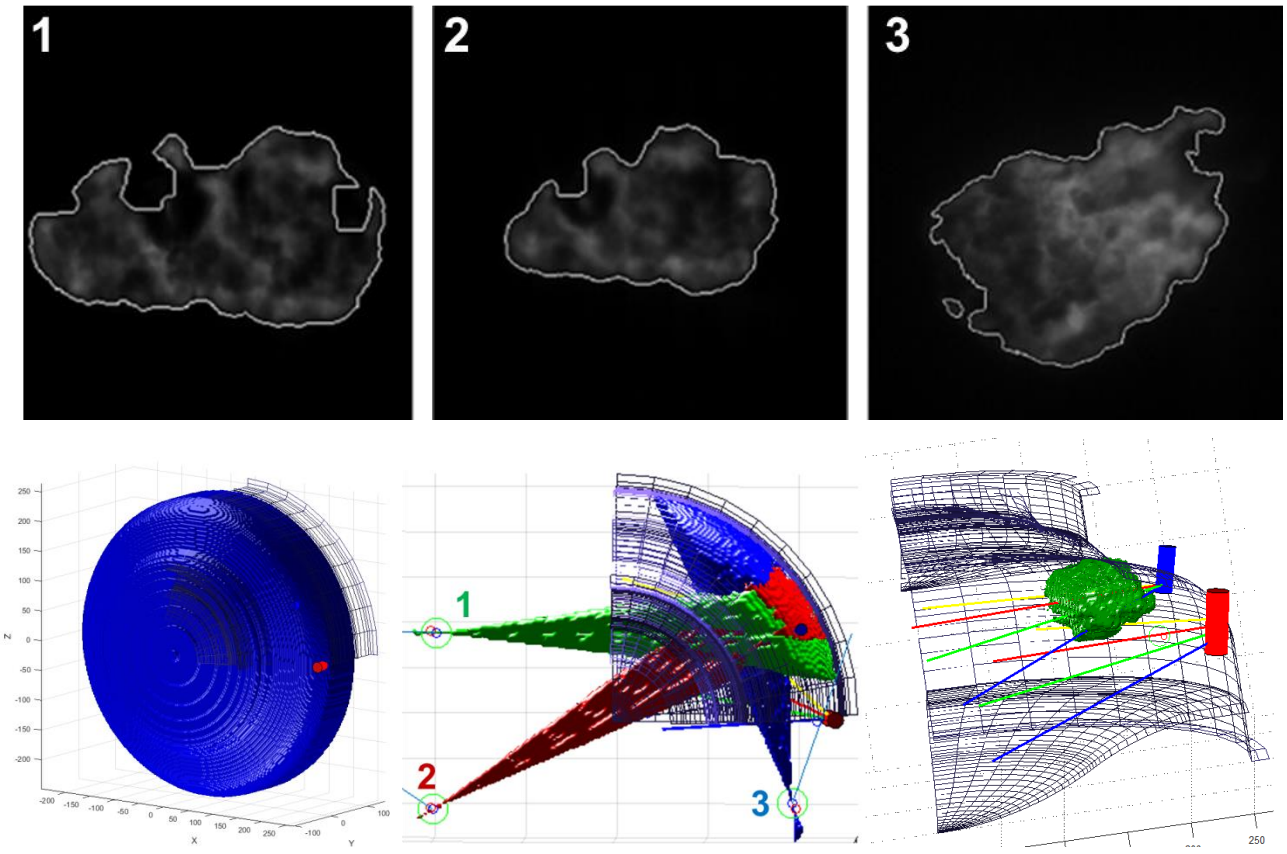

Fig. 6. Illustration of the space-carving method. Top: flame contours from the three cameras, Bottom: Cylinder voxels, cones carved from the three camera contours, and resulting carved flame volume.

3.2.4 Diesel operation

A flame ignition and propagation event captured by the three cameras is shown in Fig. 7. The spacing between consecutive images in a sequence is 100 μs, which corresponds to 0.067 CAD, but only every 7th frame is shown here. The cylinder conditions at start of injection correspond to 75% load. The first light, which is indicative of ignition, appears around -0.8 CAD after top dead centre (ATDC). After the 46th frame (around 3 CAD after ignition) the flame leaves the view of camera 3 in the top left corner.

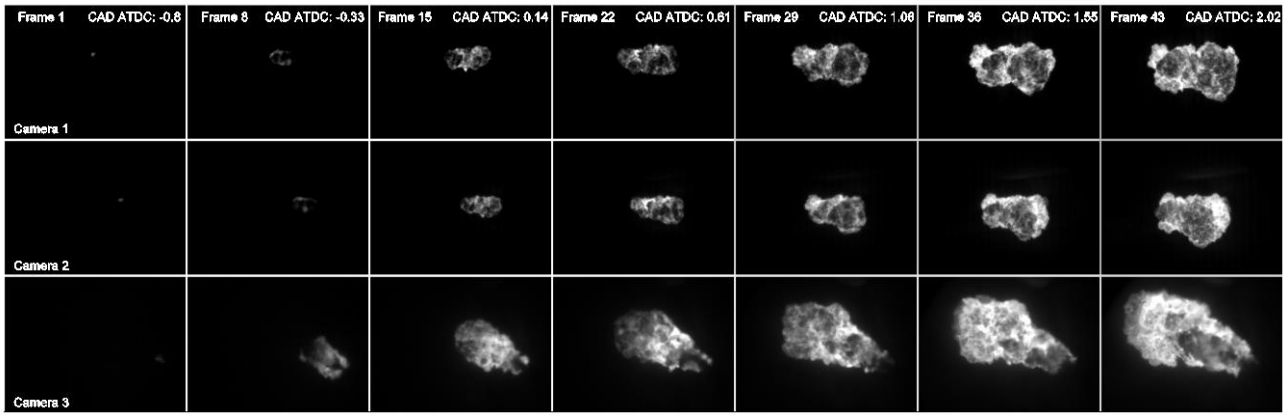

Fig. 7. Flame evolution in a single cycle as viewed from the three high-speed cameras (diesel operation).

The space carved flame development, based on the images in Fig 7, is illustrated in Fig. 8. Here every 5th frame is shown. The flame is observed to propagate in a slightly downward direction, roughly following the nozzle hole directions, while simultaneously expanding sidewise.

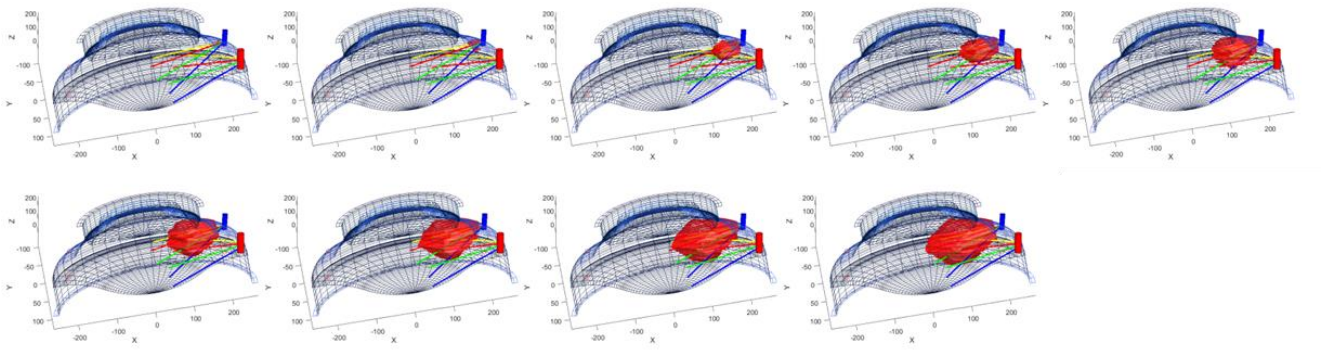

Fig. 8. Evolution of diesel flame in a single cycle, carved from the high-speed movie shown in Fig. 3. Diesel fuel injector shown in blue and gas fuel injector shown in red, lines indicate injector nozzle hole directions.

From the first frames one can gain information on the ignition process. A visualisation of the spatial location of the first ignition kernels with respect to the fuel injector and the nozzle hole directions is shown in Fig. 9. The left image displays the contour corresponding to 25% probability of observing flame emission from the region. The 3-D PDF serves to illustrate the capability of the multi-camera imaging approach of spatially locating data inside the engine cylinder. It appears that the fuel jet most is most likely to ignite towards the top of the fuel jet plume and towards the left (seen from the front). This is not unexpected as the top is closest to the exhaust valve, which is the warmest component in the combustion chamber for this type of engine. Furthermore, the left side is the side that is shielded from the strong swirling in-cylinder air flow.

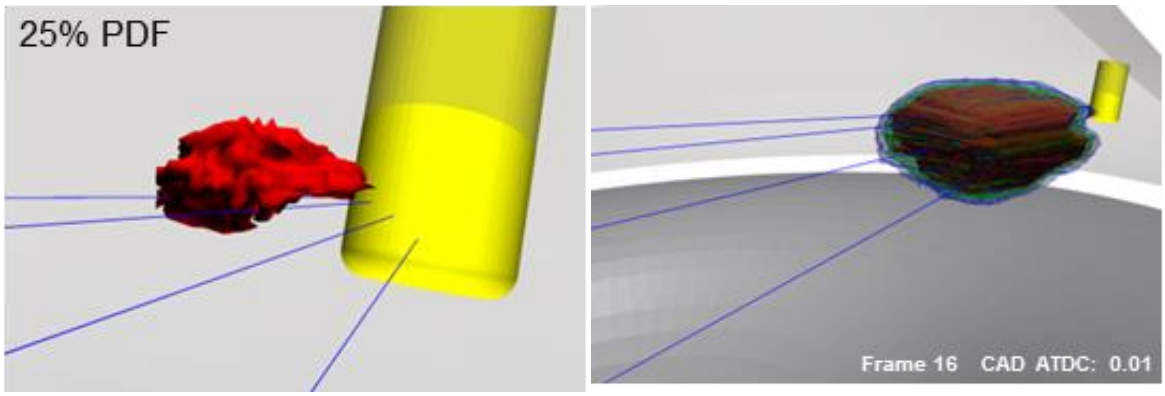

Fig. 9. Left: PDF of initial ignition location (25% probability). Right: PDF iso-surfaces of flame locations (blue: 25%, green: 50%, red 75%) illustrating cycle-to-cycle variations in flame propagation and extent.

The cycle-to-cycle variations of the propagating flames are illustrated using the 3-D PDF shown in Fig. 9 (right). The PDFs corresponding to 25%, 50% and 75% probabilities are overlaid as semi-transparent shells. The relatively small difference between the spatial extent of the 25% and 75% shells demonstrates that the cycle-to-cycle variations in flame location and propagation speed are quite small once the diesel flame has developed.

It is possible to deduce some relevant information on flame propagation from the space carved contours. In Fig. 10 the evolution of the flame length is plotted (blue line). It has been calculated as the furthest distance from any point on the individual carved contour to the fuel injector nozzle hole exits. The error bars indicate the cycle-to-cycle variations. The flame can be followed until it reaches a length of around 200 mm, after which it leaves the view of camera 3. At this time the heat release rate (red line) has reached about one third of its maximum value. The highest and lowest positions of each individual flame (with respect to the plane spanned by the nozzle hole directions) can also be quite accurately captured here (dotted black lines), from which the maximum flame height can be calculated (solid black line). It is seen to reach a height of around 100 mm before it leaves the view of camera 3.

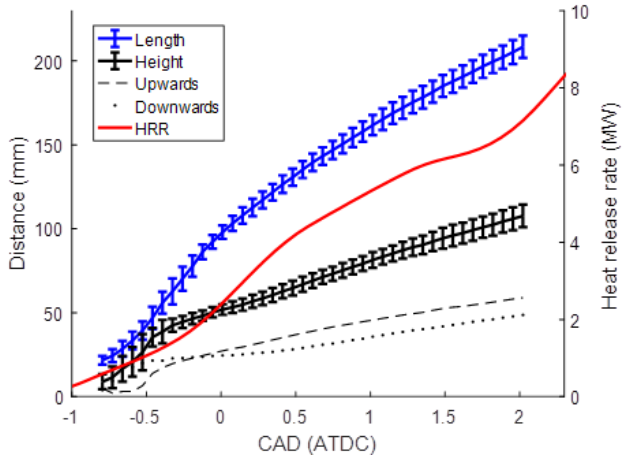

Fig. 10. Flame length and height calculated from carved voxels, up- and down-ward extents (from injector nozzle hole plane) are also plotted.

3.2.5 Natural gas operation

The tri-camera set-up was also applied to study flame structure under natural gas operation of the 4T50ME-X engine. In Fig. 11 the three high-speed sequences recorded by the cameras are shown, where high pressure natural gas is directly injected using the dedicated gas injector. The low luminosity of the gaseous flame, compared to the diesel flame is obvious when comparing to Fig. 7.

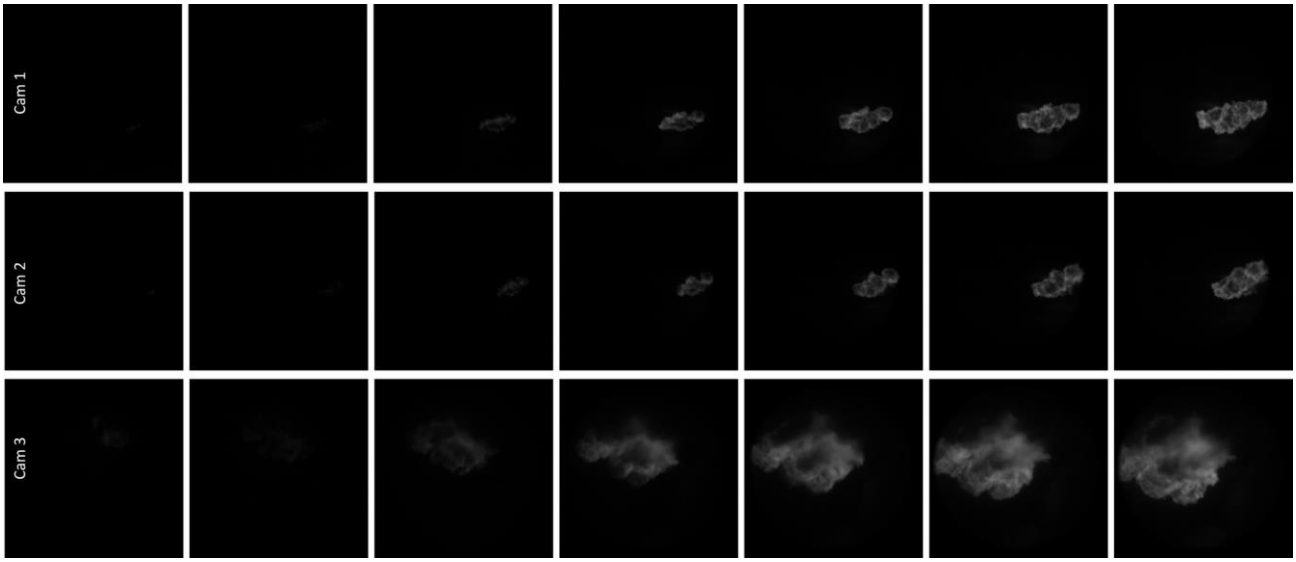

Fig. 11. Flame evolution in a single cycle as viewed from the three high-speed cameras (natural gas operation).

The space carved gas flame development, based on the images in Fig 11, is illustrated in Fig. 12. Here every 5th frame is shown.

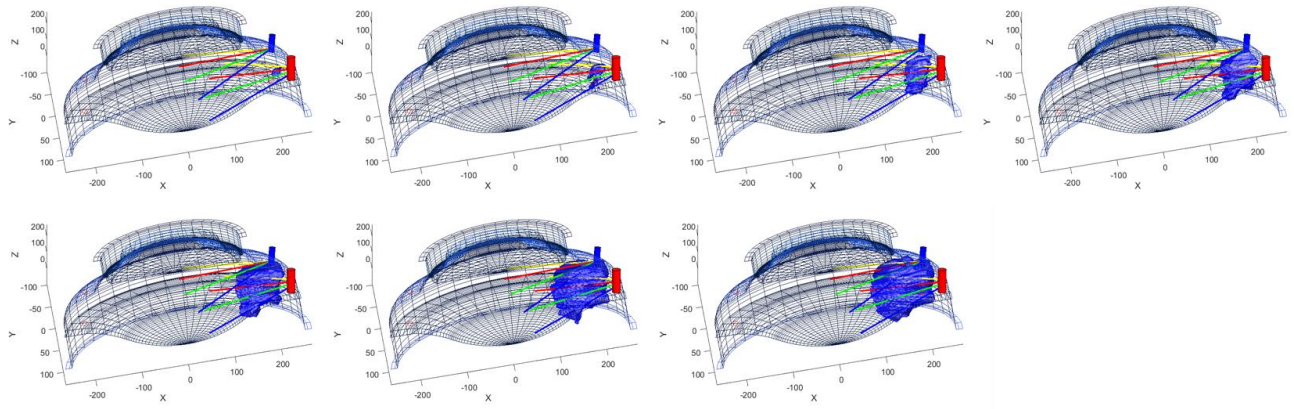

Fig. 12. Evolution of natural gas flame in a single cycle, carved from the high-speed movie shown in Fig. 3. Diesel fuel injector shown in blue and gas fuel injector shown in red.

A direct comparison between Fig. 8 and Fig. 12 illustrates that the multi-camera imaging approach is a useful tool for spatially mapping flames inside the engine cylinder. This is particularly valuable in asymmetric systems, such as the engine studied here which features multiple injectors fuelled by different fuels. The spatial location of the flame and its evolution with time form valuable information for validation of CFD models. It could also be valuable for an experimental localisation of heat-loads, where points of contact or close proximity between the flame and walls can be identified.

The use of only three cameras limits the capabilities of localising some parts of the flame accurately. By additional cameras a higher accuracy in the space carving could be achieved. Nevertheless, in the present three-camera configuration properties like flame length and flame height, or locations of ignition kernels can still be extracted reasonably accurately. One way of

achieving a large number of views could be to use an engine cover with a large number of optical ports instead of the more limited borescope access employed here.

3.3 Schlieren Imaging

3.3.1 Introduction

Normally, density variations are invisible to the human eye, until a background pattern is placed behind them, or light traverses through them and the refraction can be observed. The Schlieren technique, along with the Shadowgraph technique, is an optical method that can visualize and evaluate density variations in fluid flows. These techniques have been constantly evolving during the last two centuries by many scientists and have greatly contributed to our knowledge on aerodynamics, particularly in understanding shock waves and supersonic flows. This imaging technique is also applicable in flames and evaporating sprays and it is possible to derive parameters such as temperature, accurate liquid length. Combined with high speed imaging it becomes a powerful tool that can temporally resolve highly transient phenomena such as a diesel spray injection. An added benefit of the technique is that, depending on the Schlieren setup, the images acquired contain signal only from the density gradients, contrary to normal imaging where multiple signals can be convoluted.

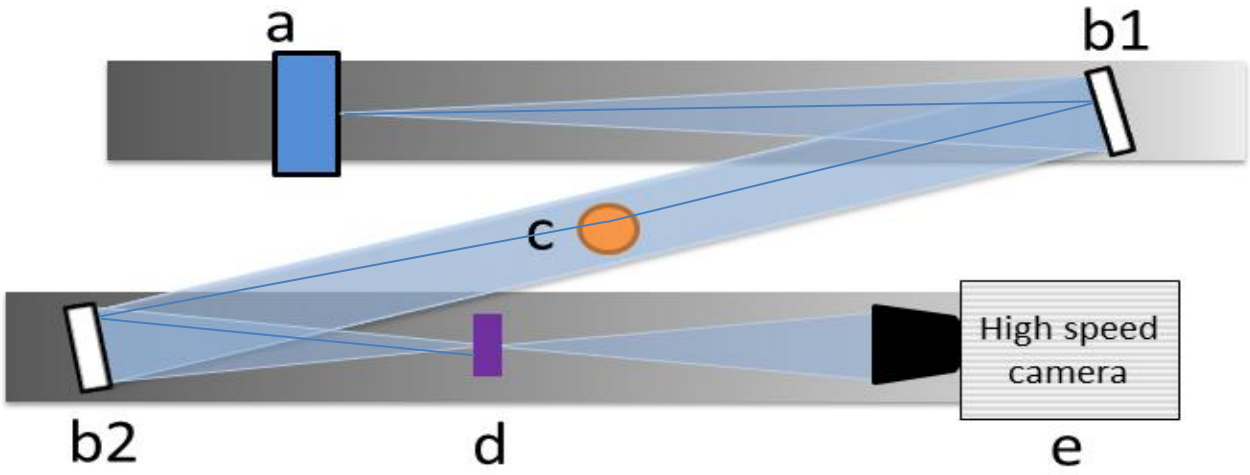

Figure 13: Sketch of the Z-type, High-speed Schlieren setup used for laboratory testing. It consists of a laser diode (a), two parabolic mirrors (b1 and b2), the gas inhomogeneity (c), the cut-off filter (d) and a high speed camera (e). A possible deflected light ray is shown for illustration purposes only.

Ideally, the light source should be a very bright, point source of light, infinitely small that creates diverging rays. If these rays pass through a converging lens (b1 in Fig. 13) they will exit as parallel rays forming a column of parallel light (collimated), as long as the source is positioned at a distance equal to the focal length of the lens used. If another lens is placed in the path of this collimated column of light (b2 in Fig. 13), it will converge towards a focal point, at a distance defined by the focal length of the lens that was introduced. At this stage, an exact image of the

light source will be formed and the setup seems pointless. However, the focal point of a lens is mathematically described as a Fourier transformation of the image that the lens received. In the Fourier plane, the intensity values that comprise the original image are translated to frequencies. If all light is collimated and the light source is infinitely small, only one frequency component will be present and appear as a round dot (Fig. 14). By introducing a cut-off, some of these frequencies will be blocked, leading to a different final image. If this cut off is a sharp opaque plate that is positioned so that half the Fourier plane is blocked, the intensity of the final image will be half of the original due to half the frequencies being blocked. Nevertheless, rays that escape collimation due to a disturbance will also be part of the Fourier plane as a component spatially placed outside the round dot, since they are not part of the parallel light. This new component will either escape the cut off that was introduced, or will be blocked, leading to a brighter patch in the final image or darker respectively. At this point it becomes clear that the detection of the density gradients is performed based on the intensity variance from the undisturbed image. Other forms of cut offs will provide different results based on the filtering that takes place in the Fourier domain. Obviously, absorbing or reflecting media will block light and appear perfectly dark in the final image.

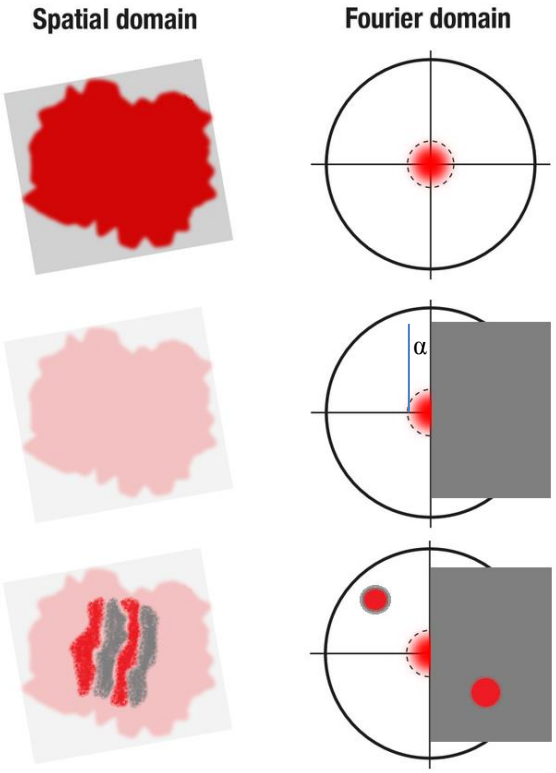

Figure 14: Illustrative final images and their corresponding Fourier images. In the cases where collimation is perfect, one component exists in the Fourier domain and the cut-off will simply dim the image. When other frequency components exist due to disturbances, the density gradients will be visualized as brighter or darker regions in the final image.

One compromise of the Schlieren setup is the trade-off between sensitivity and measuring range. As long as the cut-off is perfectly opaque, the deflected rays that are blocked from the cutoff will appear perfectly dark on the reconstructed image or perfectly bright if they escape the cutoff. If it is necessary to increase the measuring range, a number of measures can be taken, in the expense of lower sensitivity. By increasing the size of the light source, a less defined focal point is formed at the Fourier domain, less light will be collimated and therefore, more of it will escape the frequency filtering. Another way would be to use a graded filter cut-off instead. The gradation length defines the measuring range of the setup, meaning that a longer gradation will provide low sensitivity with high measuring range and conversely, a short gradation will have high sensitivity as in the case of a completely opaque cut-off but with poor measuring range. The cut-off positioning is also important in this trade-off since it defines which components are filtered first. By gradually introducing the cut-off in the Fourier domain, the required sensitivity is achieved. However, the system response becomes non-linear away from the 50% position, especially below 10% or above 90% positions.

The Shadowgraph technique is very similar to Schlieren imaging since the detection of gradients again relies on the rays that escape collimation and provide a contrast ratio proportional to the deflection. The cut-off filter is removed and the second lens can be removed since it is redundant (Fig. 15). Essentially, the only requirement is a light source to provide collimated light, thus the experimental setup is much simpler and easier to use.

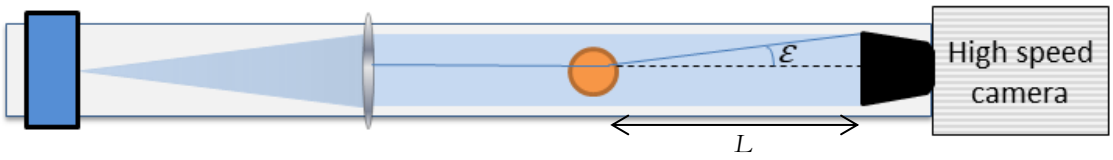

Figure 15: Illustration of a high-speed Shadowgraph setup. Here, mirror b1 is replaced by a converging lens in order to collimate the diverging light from the point light source. The ray deflection angle ε is shown exaggerated and L corresponds to the distance between the disturbance and the camera.

Since these imaging systems rely on pure geometrical optics principles, the governing equations are relatively simple. By knowing the geometry of the Schlieren or shadowgraph optical setup, the deflection angles can be calculated and the density gradients that caused them can be derived. For air and other gases the refractive index n and gas density ρ are related according to:

$$n - 1 = k\rho \qquad (4.3.1)$$

where k, the Gladstone-Dale coefficient. In many cases the pressure, temperature and density are related by the ideal gas law:

$$\frac{p}{\rho} = RT \qquad (4.3.2)$$

where R, the ideal gas constant. It can be shown that optical inhomogeneities refract light rays proportionally to their refractive index gradients and the resulting ray curvature is given by:

$$\frac{\partial^2 x}{\partial z^2} = \frac{1}{n}\frac{\partial n}{\partial x}, \qquad \frac{\partial^2 y}{\partial z^2} = \frac{1}{n}\frac{\partial n}{\partial y} \qquad (4.3.3)$$

where x and y are the Cartesian coordinates corresponding to the direction that the gradient deflected the ray on the image plane. By integrating along the optical axis (z direction), the ray deflection angles ε become,

$$\varepsilon_x = \frac{1}{n}\int \frac{\partial n}{\partial x}\partial z, \qquad \varepsilon_y = \frac{1}{n}\int \frac{\partial n}{\partial y}\partial z \qquad (4.3.4)$$

and for a disturbance extent of L along the optical axis the equations become,

$$\varepsilon_x = \frac{L}{n_0}\frac{\partial n}{\partial x}, \qquad \varepsilon_y = \frac{L}{n_0}\frac{\partial n}{\partial y} \qquad (4.3.5)$$

In the case of the Schlieren system, if we use the small angle approximation ($tan\varepsilon \approx \varepsilon$), a ray displacement of $\Delta\alpha$ at the cut-off position will be described by:

$$\Delta\alpha = \varepsilon F \qquad (4.3.6)$$

where F the focal length of the second lens. If the light source is uniformly bright, the *image contrast* ($\Delta I/I$), or equivalently the sensitivity, will be given by:

$$\frac{\Delta I}{I} = \frac{\Delta \alpha}{\alpha} \qquad (4.3.7)$$

where α the size of the source's image on the focal point (Fig.14). Combining the above we obtain:

$$\frac{\Delta I}{I} = \frac{\varepsilon F}{\alpha} \qquad (4.3.8)$$

From this simple equation it is easy to notice that the sensitivity of the setup will rely on the size of the source and the focal length of the second lens.

Modern methods for Schlieren imaging are less complicated and rely mostly on computational methods. Background Oriented Schlieren (BOS) is a technique that only needs a camera and a characterized background image. The background image is used in order to obtain reference points across the image and when a disturbance is introduced, the reference points are retraced in the new image. Due to the density variations, the background points will have moved slightly between the two frames and this movement can be evaluated by comparing the images. A cross correlation algorithm, which is typically used in Particle Image Velocimetry (PIV) measurements, can be used in the same manner so that the displacement vectors are obtained. The vectors will contain information on the magnitude of the disturbance and the directionality as well. In other words, with just two images, all of the necessary information is obtained without the complexity and precision required in typical Schlieren systems. This technique has been used in large scale applications such as helicopters, ventilation hoods, etc. where a Schlieren optical setup is impossible to install or extremely expensive since it would require big mirrors and strong light sources. This method is becoming increasingly popular and a lot of related work has been published in recent years. The most important aspects of this method are the background pattern and the distance of the schliere (disturbance) relative to the background. The background pattern most commonly is comprised of dot patterns, randomly generated, big enough to be detected but small enough to offer high spatial resolution. In cases where a laser light source is used, a speckle pattern is formed due to the interaction between the laser's coherent light and the camera sensor or the projection screen. This usually undesirable effect creates an ideal dot pattern that can be used as a background image for BOS. A natural background can also be used for BOS but the reference points and the evaluation of their displacement becomes more difficult.

3.3.2 Experimental results with Schlieren techniques

A modular Z-type Schlieren setup was devised for the purposes of this project. A 2 Watt, 452nm laser diode was used as the light source, since it can be found at very low cost and produces high power, coherent and narrowband light. The laser diode was coupled to a 600μm optical fiber in order to provide a physically small light source that provides a circular diverging beam, thus providing an ideal light source for a Schlieren application. Other configurations were tested as well, with diffuser lenses in front of the laser diode that essentially reduce the coherence and scatter light, leading to an extended source and a more uniform background, thus increasing the dynamic range of the setup. Two 75mm diameter parabolic mirrors with a focal distance of 500mm were used in order to collimate and refocus the laser light. Mirrors are preferred over lenses, since they don't introduce aberrations and they are readily available in big sizes. A Photron SA-5 high speed camera was used to obtain the Schlieren images since the purpose was to characterize the injection and combustion inside the 4T50ME-X test engine with the optical cover fitted that allows for a view straight through the combustion chamber. All the components were mounted on two flat aluminum beams with sliding carriers for quick and secure positioning. Thus the whole setup can be moved to the measurement location, pre-aligned, with only minor adjustments necessary.

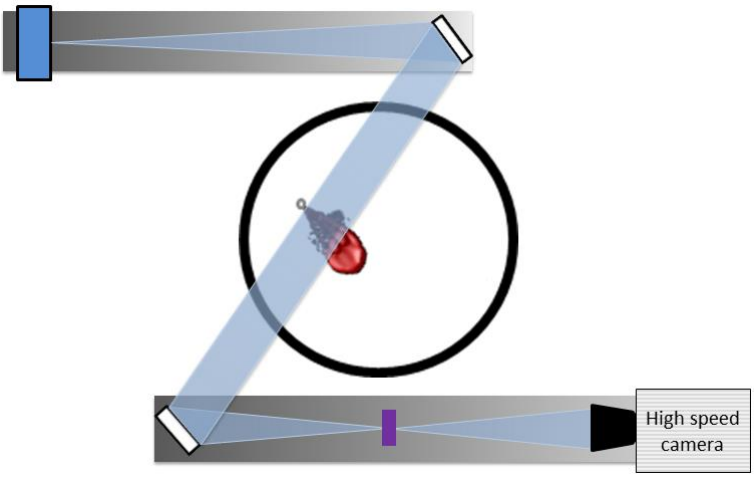

Figure 16: Sketch of the potential layout when measuring in the actual engine. Alternatively, lenses can be used instead of mirrors to create an in-line setup.

While testing in laboratory conditions, a Bunsen burner was used with a mixture of propane and butane as fuel in order to obtain a flame and thus a source of density gradients similar to a flame inside the engine. Results can be seen in Figure 17. Noticing the shadowgraph image (a), only the edges of the flame are discernible as bright or dark streaks. The image looks relatively flat and the only information that can be obtained are the flame edges. However, on the Schlieren images, the contrast contours are obvious across the whole flame and the image has added depth, giving almost a three-dimensional effect. The thermal gradient of the flame is imaged correctly across the whole flame volume. In fact, in image b of figure 17, the density gradients of the interface between atmospheric air and the outer flame edge is strong enough to overwhelm the measurement range of the setup, as is apparent by the uniformly dark region around the flame base indicated by the arrow. In image c of the same figure, a 1500grit ground glass diffuser lens is placed in front of the light source. The diffuser increases the physical size of the source, thus reducing the sensitivity of the setup, while increasing the dynamic range over which the setup can resolve density gradients. The thermal gradient is resolved more accurately, without totally dark regions that would cause loss of information. The speckle pattern is somewhat attenuated and a more uniform background

is observed. In image d, the diffuser lens was exchanged to a 120grit ground glass. The higher roughness of the surface scatters light even more compared to the 1500grit diffuser, thus further increasing the measurement range of the setup. While increasing the roughness, the speckle pattern becomes even less obvious since the coherence of the laser light is attenuated further. While using diffuser lenses increases the dynamic range, a great amount of light is lost due to the scattering. This can be problematic since, usually 50% of the initial light is either way lost at the cut-off and additionally, the dynamic range is dictated by the final background luminosity.

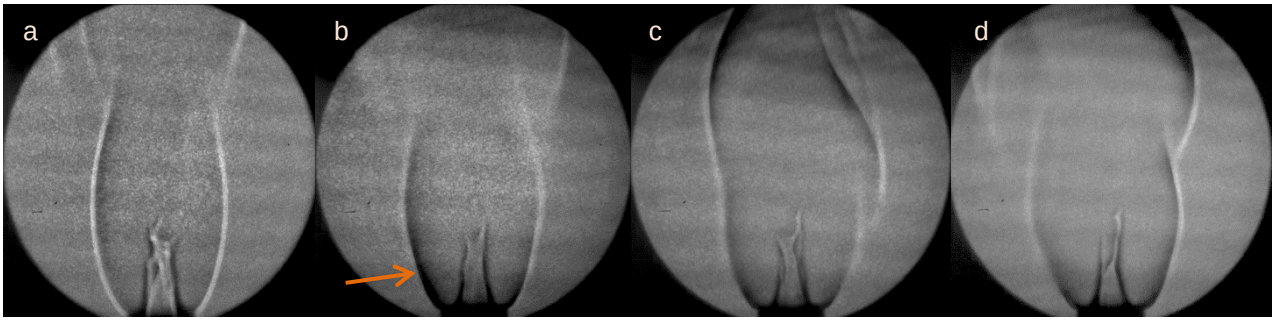

Figure 17: (a) A typical shadowgraph image where the flame appears flat. Only the furthest edges of the flame and the core with the unburnt gases are apparent as bright and dark regions respectively. (b) Schlieren image obtained with an aperture used as the cut-off. The increased image contrast is obvious compared to the shadowgraph image and the image seems to have an added depth. (c) A 1500grit ground diffuser lens is added. The diffuser increases the size of the source, thus reducing the sensitivity of the setup while increasing the dynamic range. (d) The diffuser lens used was a 120grit ground glass. The higher roughness further increases the measurement range of the setup. Notice also the attenuated speckle pattern on the background.

However, the laser diode that has been used is powerful enough that despite the diffuser and the losses at the cut-off, neutral density filters with total OD 4 were necessary in order to avoid saturation of the camera, even at the minimum exposure of 370ns. This is very encouraging for the test on the engine since it shows that it has the potential to cope with much harsher environments, such as the test engine, where soot deposits on windows and absorbing media might pose a challenge for other light sources.

In addition to above Schlieren imaging, the concept of Laser speckle-Background Oriented Schlieren (BOS) was tested. The optical setup used was the one shown in Figure 15. A spherical f=+200mm lens was used to collimate light from the same laser diode and the high speed camera was positioned directly in the path of the parallel light. The laser power was kept low which provided a more pronounced speckle pattern. In principle, this optical setup is used to create Shadowgraph images. However, the detection of the density gradients is not based on the contrast or the brightness of the image regions anymore. Instead, the motion, or the changes in the speckle pattern are evaluated over a background image that doesn't have any disturbances. The rays that create the speckle pattern will be the same, however, they will be deflected to a different position due to the density gradients. When comparing to the background image, the displacement of the speckles can be evaluated by direct cross correlation. Results are shown in figure 18. Frame a is the background image taken without any schliere present. Frame b includes a gaseous fuel plume rising above the burner. No discernible difference is noticed by naked eye,

the speckle pattern is prominent and no density gradient is obvious. In frame c, the use of a high-pass filter is demonstrated. After this operation, the image looks almost identical to a typical PIV

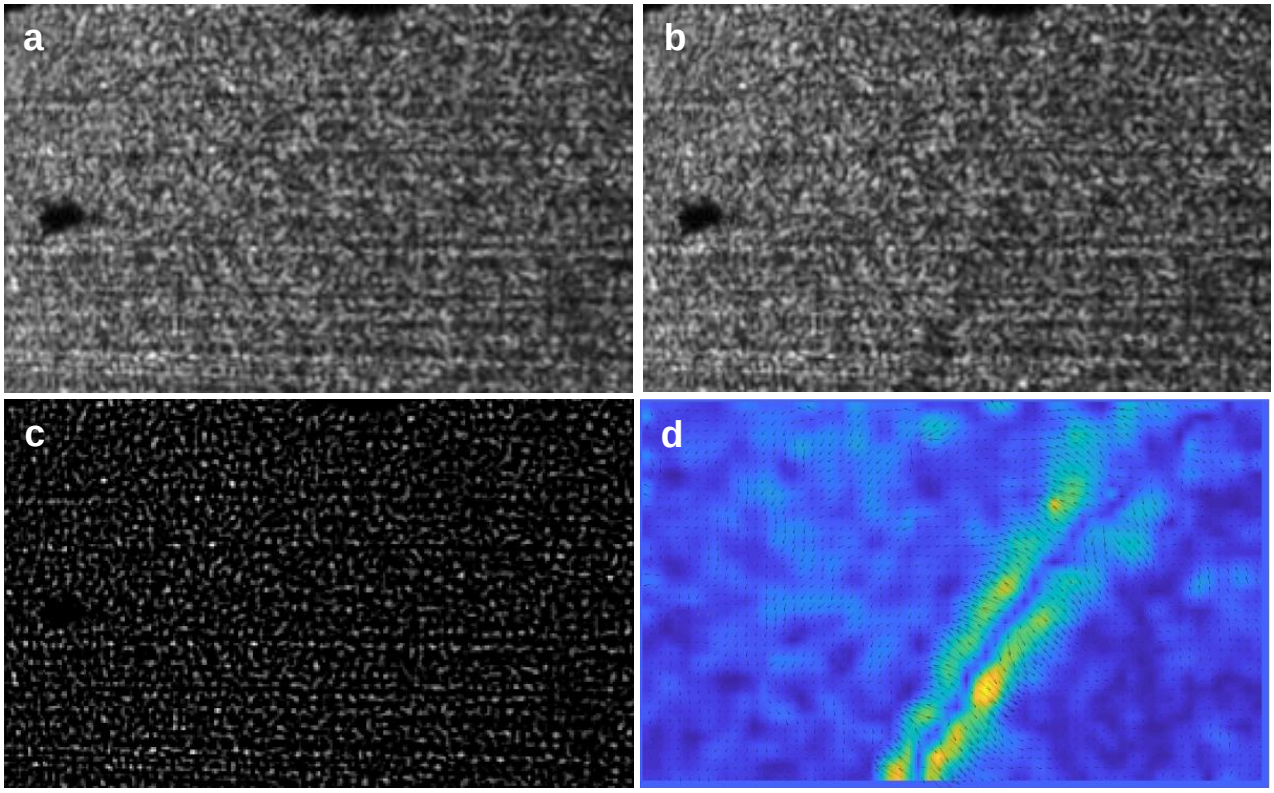

Figure 18. Frames (a) and(b) are the background image and the schliere image respectively. No significant difference is obvious. Frame (c) demonstrates the use of a 5x5 pixel high-pass filter in order to make the speckle pattern more obvious. Frame (d) shows the final result from the cross correlation. The magnitude of the density gradients is shown color graded and the direction is shown by the black arrows.

image. A 5x5 pixel high-pass filter was used in order to obtain this image and make the cross correlation easier. Frame d shows the final image, where the color grading demonstrates the magnitude of the speckle displacement and the black vectors show direction as well. If the system is calibrated using a characterized target, the image ratio is known and thus the displacement can be obtained in millimeters. If the disturbance is well localized, as is the case with a stationary burner, the distance to the camera sensor is known and the deflection angle can be calculated according to equations 4.3.1-4.3.5. Therefore, the density gradients can be derived from the same equations. In other words, with a single frame and a reference image the density gradients can be characterized in both magnitude and direction. This is a simpler and more robust approach compared to traditional Schlieren imaging. Sensor non-linearities do not intervene with the measurement and no cut-off is present that would reduce the light intensity and define the sensitivity of the setup. If quantitative results are needed in conventional Schlieren systems, a calibration is necessary to correlate light intensity with the $\Delta\alpha$ displacement at the cut-off, something that is avoided with a BOS system. However, in speckle pattern BOS, the sensitivity of the setup relies on the speckle size which is not directly adjustable and depends on the interaction with the sensor. If higher resolution is necessary, the distance L between schlieren and camera can be increased.

3.4 Lubrication Oil Visualization

3.4.1 Introduction

Engine lubrication is very important for engine sustainability and efficiency. It becomes even more important when heavier fuel types who contributes to lubrication are changed to alternative fuel without the same lubrication abilities. Consequently, the efficiency of the lubrication system, and more specifically, the distribution of the lubricant inside the engine, becomes of high importance. One wants to be sure that the lubricant oil reaches all the important and needed sites inside the engine. However, the performance of the lubrication systems sometimes can be very hard to study in real time due to hostile environments inside engines, specialized techniques are required to facilitate in situ measurements.

The in-cylinder visualization of lubricant oil can be studied using a variation of LIF (Laser induced fluorescence) technique that revolves around shining laser light inside the engine to receive back an emission signal from an excited fluorescence dye that has been applied to the lubrication oil. This received signal will then tell us about the current position of the lubricant oil and the sites it reaches. Furthermore, the use of LIF has some benefits as a detection technique, such as the ability to measure non-intrusively while the engine is running, enabling a realistic measurement environment. A reason for applying the fluorescence dye to only new oil coming into the system is to be able to monitor its injection together with its dispersion and mixing with the oil already present inside the engine.

This part of the diagnostics work aims at identifying a suitable fluorescence dye for use in LIF (Laser induced fluorescence) experiments to trace lubricant oil inside marine engines. To be considered suitable as oil tracer, the fluorescence dye must have a strong quantum yield, be compatible with temperatures normal for a marine engine liner and perturb the lubricant oils characteristics as little as possible.

Several potential dye candidates have been selected for investigation based on previous research in the similar fields. These dyes are then evaluated in a laboratory environment using a Class IV laser, Nd-YAG frequency doubled (532 nm), for the LIF excitation process. The choice of using a wavelength of 532 nm was made to reduce the amount of fluorescence from the oil itself as the oil will fluorescence much more if shorter wavelengths would be employed. The experimental setup used was capable of simulating the temperatures present inside a marine engine cylinder liner. The tracer species were studied with focus on solubility, intensities and temperature resistivity. Thereafter, the most suitable candidates are chosen for their possible usefulness in 2-D imaging of oil distribution inside the engine.

3.4.2 Experimental Setup

Excitation Laser

The experimental setup was created with the purpose to determine the fluorescence efficiency of the individual dyes at temperatures realistic to actual marine engines. The used light source was a

Q-switched Nd-YAG laser (model: Quantel Brilliant-b), configured to produce light at 532 nm and 355 nm. The fluence for the two respective pulse energies are shown in Table 4.1, they are calculated for an unfocused laser beam.

Table 4.1: List the used wavelengths with their respective maximum fluence, the values assumes the use of maximum laser energy for respective wavelength and an unfocused laser beam with beam diameter of 10 mm. The corrected fluence is achieved after multiplying the fluence with a factor of $N^{0.25}$, where N is the

Wavelength	Fluence	Corrected Fluence
355 nm	$1.9 \cdot 10^3 J/m^2$	$5.9 \cdot 10^3 J/m^2$
532 nm	$3.8 \cdot 10^3 J/m^2$	$10 \cdot 10^3 J/m^2$

The choice of focusing mainly on excitation by 532 nm light was made mainly due to the lubricant oil having a stronger fluorescence emission at shorter wavelengths. However, one must be aware that good candidates at other excitation wavelengths might exist.

Optical setup

A graphical representation of the experimental set up is shown in Figure 19. The beam was aligned onto the sample using one dichroic mirror together with a quartz beam splitter to reduce the fluence.

Thereafter the beam went through an aperture, which blocked the Gaussian wings, in order to achieve a more homogenous top hat profile.

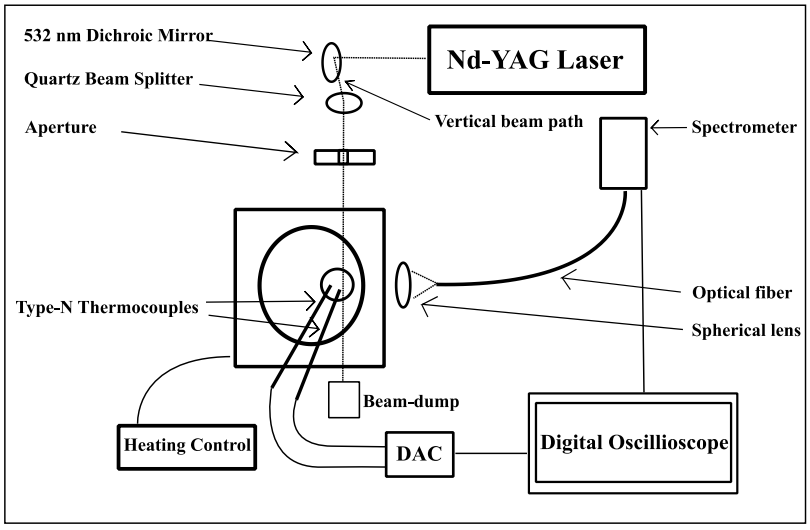

Figure19: Schematic view of the experimental set up.

Sample preparation and placement

Each sample was prepared in a ventilated cabinet, the dye concentration was measured using a scale with a precision of 0.001 g and the oil quantity was measured by pipettes, with a precision of approximately 0.5 ml. Thereafter the oil was heated up to 40°C in an ultrasonic bath for approximately 10 minutes to improve mixing.

During the measurement, the oil sample was kept inside an Erlenmeyer flask made of clear Duran® glass, this flask type is highly thermal resistant and possess low absorption of maximum

10 percent in the spectral range of 350 up to 2000 nm. The heating of the sample was performed by a circular heating plate, able to increase the temperature of the sample to 150°C. The temperature range was chosen to cover the normal marine engine liner temperatures of 75-125°C.

Signal and temperature acquisition

Using a spherical lens with a diameter of 50 mm and a focal length of 60 mm the fluorescence signal from the sample was directed onto an optical fiber cable connected to a spectrometer. The fiber was intentionally placed at a 90° angle relative to the laser beam path to minimize the light from the laser reaching the spectrometer. The spectrometer had a resolution of 1.10-1.30 nm.

For measuring temperature, two individual thermocouples of type N were used. The Type-N thermocouples are made out of a Nicrosil and Nisil alloy, with an approximate uncertainty of 1.5°C in this temperature range. These were connected to a DAQ card which transferred the signal to a digital oscilloscope running LabVIEW. The laser energy was evaluated separately using a pyroelectric sensor without diffuser connected to a universal power meter that logged the data.

2D – Imaging set up

The imaging set up (Figure 20), is similar to the previous setup with some small modifications. A

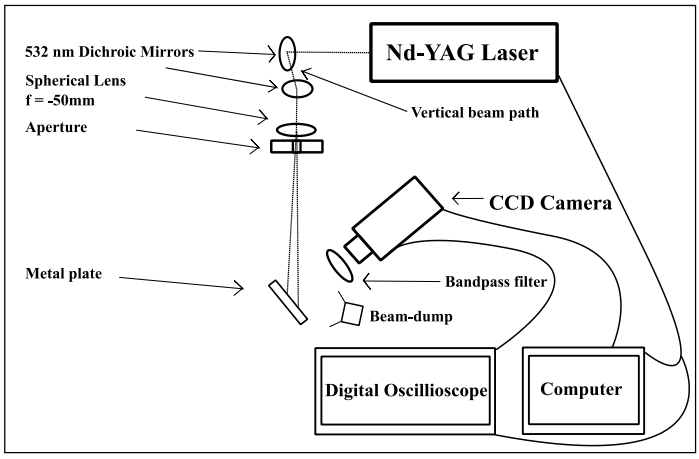

Figure 20: Schematic view of the 2D imaging setup.

spherical expansion lens of focal length of -50 mm was added before the aperture, to illuminate an area of approximate 80 cm^2 on the metal target. The target itself was a metal plate covered with a thin layer of neat lubricant oil. During the measurements, a small amount of dye traced lubricant oil was introduced and allowed to move over the plate. Pressurized air was later blown on the metal palate to simulate movement in arbitrary directions.

The imaging was done using an intensified CCD camera (ICCD model: ANDOR iSTAR). For the 2D imaging, the studied dye was Pyrromethene 650. Therefore an optical bandpass filter; centered around 589 nm with a FWHM of 10 nm and a diameter of 50mm, was used to allow passage of fluorescence while discriminating against scattered laser light.

3.4.3 Identifying suitable tracer species

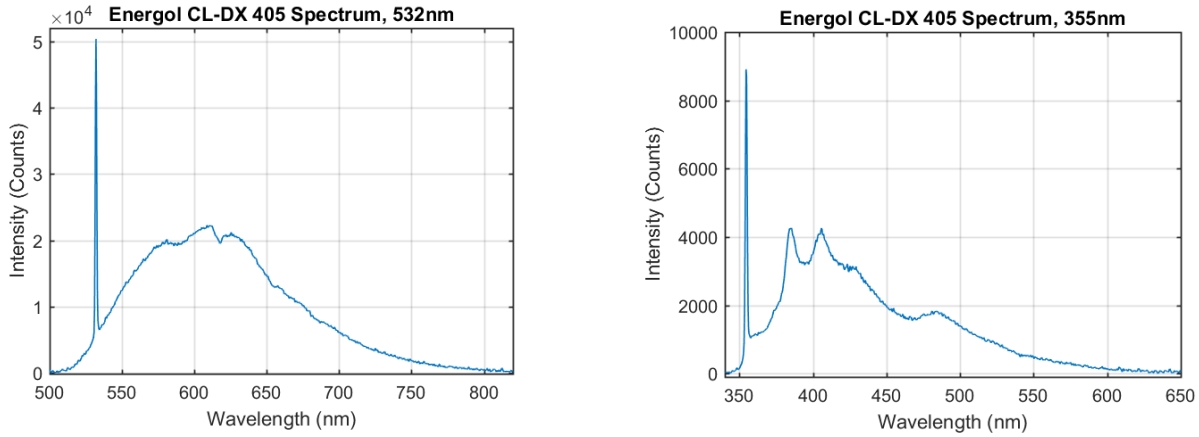

Figure 21. (a) Emission spectrum of Energol CL-DX 40 and the visible laser peak. Excitation wavelength of 532 nm and energy at 815 J/m^2.(b) Emission spectrum of Energol CL-DX 40 with an excitation wavelength of 355 nm and energy at 66 J/m^2

Lubricant oil

The lubrication oil used was Energol CL-DX 405 which is a lubrication oil specially used in marine engines and possesses a self-ignition temperature called flash point at around 190 – 230 °C [6]. When exposed to 532 nm and 355 nm light the oil gives two distinct fluorescence spectrums (Figure 21, a and b). The selected tracer dye should ideally be spectrally shifted from this interfering oil fluorescence.

Dye selection

The selected dyes are presented below with their name, chemical formula and emission spectrum. The solvent used was ethanol. Excitation was done using a frequency doubled Nd-YAG laser producing 532 nm light. The laser energy was varied to a good signal-to-noise ration and thus, promote the shape of the respective spectrum.

The dyes were chosen due to their possibility to fulfill the needs of the experiments with regards to solubility, altering of lubricant oil properties and temperature resistance. Several of the investigated dyes were selected based on previous use in similar research. When it comes to dyes their fluorescence emission strength is dependent upon temperature due to the molecules being affected by thermal collisions and vibrations. If a high enough temperature is reached the fluorescence dye will stop emitting fluorescence as the ground state is moved due to change of the molecular structure, this phenomenon is called thermal bleaching and needs to be avoided.

Rhodamine 640 Perchlorate ($C_{32}H_{31}N_2O_3.ClO_4$)

This dye is also known as Rhodamine 101 and is a proficient fluorescence dye for pulsed dye-lasers. It possesses a fluorescence peak at around 600 nm

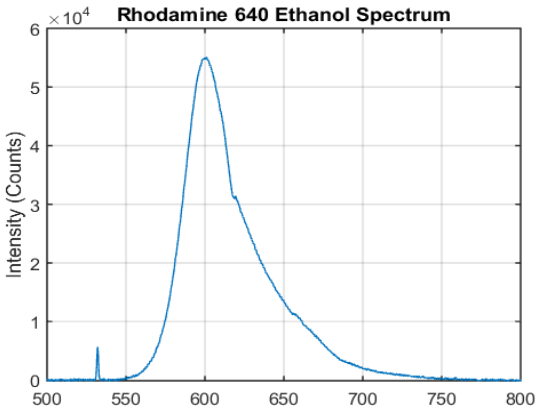

Figure 22: Fluorescence spectrum of Rhodamine 640 when solved in ethanol. Excitation wavelength of 532 nm with laser energy at 20 J/m^2

when solved in ethanol (Fig.22) and a melting point of around 210°C [1, 8, 9].

Rhodamine 590 ($C_{28}H_{31}ClN_2O_3$)

Also known as Rhodamine 6G, this dye is one of the more well-known fluorescence dyes used with Nd:YAG 532 nm pumping. It possesses an absorption maximum is around 530 nm when solved in ethanol, a fluorescence peak at around at 558 nm (Fig.23) and a melting point at around 315°C [1].

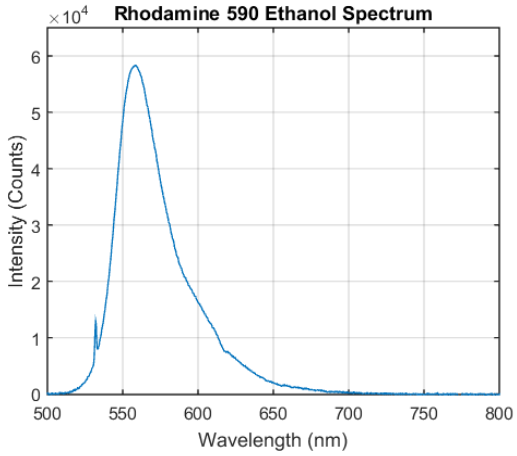

Figure 23: Fluorescence spectrum of Pyrromethene 590 dissolved in ethanol. Excitation wavelength of 532 nm with laser energy at 9.2 J/m^2.

Pyrromethene 567 ($C_{18}H_{25}BF_2N_2$)

Another well-known dye, sometimes used as an alternative to Rhodamine 590. It possesses an absorption maximum at around 518 nm when solved in ethanol, a fluorescent peak at around 544 nm (Fig.24) and a melting point at around 208-209 °C. The dye possesses a high quantum efficiency in both solid and liquid solvents has been used to do oil film measurement on piston rings.

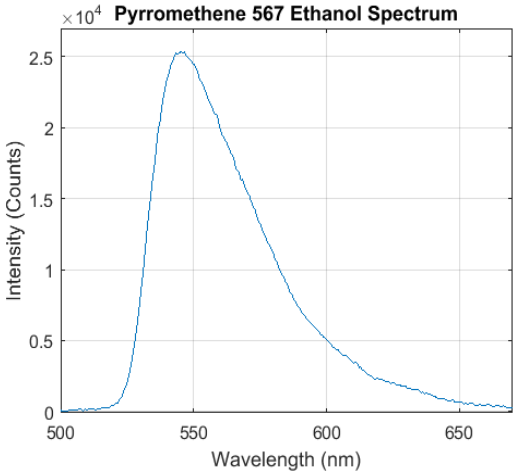

Figure 24: Fluorescence spectrum of Pyrromethene 567 when solved in ethanol. Excitation wavelength of 532 nm with laser energy at 25 J/m^2.

Pyrromethene 597 ($C_{22}H_{33}BF_2N_3$)

This dye is similar to Pyrromethene 567 but tends to have somewhat lower quantum yield efficiency due to small molecular differences, however the dye possesses a versatile solubility. It has an absorption maximum at around 525 nm when solved in ethanol, a fluorescent peak at around 553 nm (Fig.25) and a melting point at around 247 -261°C. The dye is soluble in many mediums such as ethanol, methanol, high temperature plastic and gasoline.

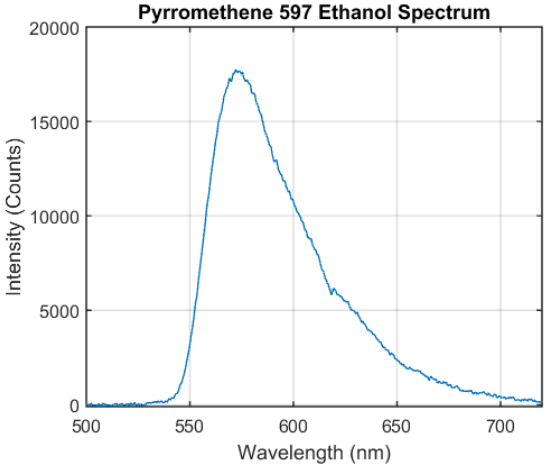

Figure 25: Fluorescence spectrum of Pyrromethene 597 when solved in ethanol. Excitation wavelength of 532 nm with laser energy at 76 J/m^2.

Pyrromethene 650 ($C_{16}H_{18}BF_2N_3$)

Being part of the Pyrromethene family, it exhibits similar aspects as Pyrromethene 567 and 597. It possesses an absorption maximum at around 590 nm when solved in ethanol, a fluorescence peak with two maximums at 614 nm respectively 620 nm (Fig.26) and a melting point at around 255-258 °C [9, 20]. Additionally, an anti-stokes peak can be seen next to the laser peak in the spectrum.

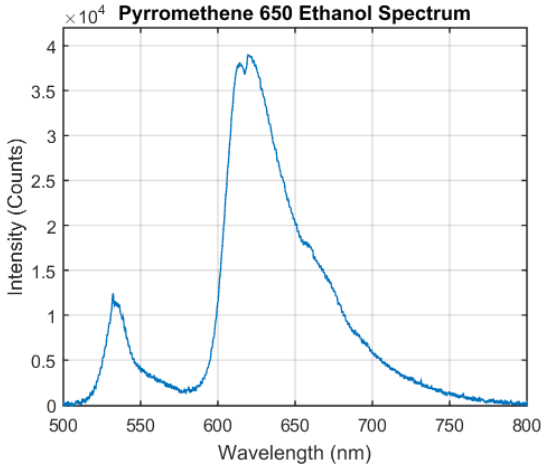

Figure 26: Fluorescence spectrum of Pyrromethene 650 when solved in ethanol. Excitation wavelength of 532 nm with laser energy a

DCM ($C_{19}H_{17}N_3O$)

This dye possesses a broad absorption spectrum and thus absorb wavelengths all the way down to 300 nm and up to 550 nm while solved in ethanol. It has a fluorescence peak with two maximums at 612 nm respectively 629 nm (Fig.27) and a melting point at around 215 -220 °C.

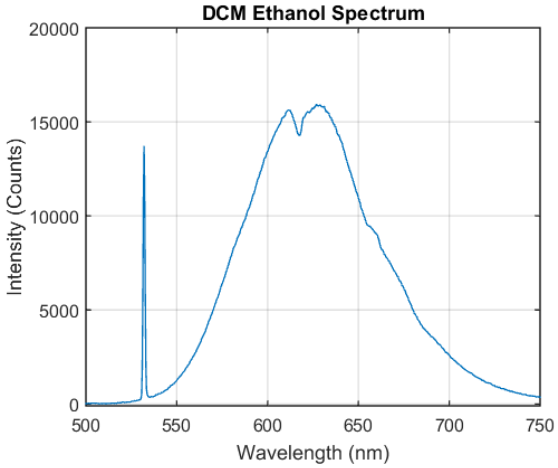

Figure 27: Fluorescence spectrum of DCM when solved in ethanol. Excitation wavelength of 532 nm with laser energy at 66 J/m^2.

Bestoil Green FYG ($NVAL$)

This dye is commonly used for oil leakage detection and is therefore usually excitable by UV light. Therefore, this dye could not be excited using 532 nm and the excitation wavelength was switched to 355 nm. It has a fluorescence peak at 510 nm when solved in ethanol (Fig.28) and a melting point at 205°C.

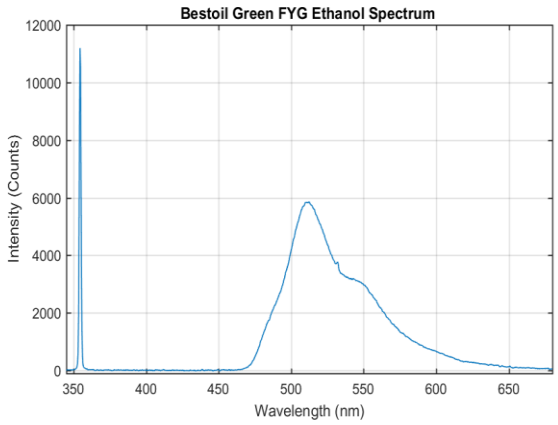

Figure 28: Bestoil Green FYG dissolved in ethanol, excitation wavelength of 355nm with energy of 15 J/m^2

3.4.4 Results

The goal was to evaluate different fluorescence dyes to be used to trace lubrication oil inside marine engines. The dyes should be soluble in the lubricant oil, resistant to temperatures of 75-

125°C, normal for these engines and to as a small degree as possible not perturb the characteristics of the oil, therefore the concentration of the dye was kept to a minimum.

Temperature resistance

The following results show the emission spectrums of each individual dye when solved in lubricant oil at increasing temperatures together with their temperature dependent intensity curve. Each measurement was taken during a small period of time were 15 spectrums of the same temperature was averaged into the final one shown in the result. During this time the temperature was slowly increasing but stayed well within the deviation range for the thermocouples at 1.5 °C.

Pyrromethene 567

The spectrum of this dye shows significant overlap with the lubricant oils own spectrum, however, with a much higher intensity (Fig.29). The laser fluence was averaged around 18.8 J/m^2 with a dye concentration of 0.025 g/L.

Pyrromethene 567 had an almost constant decrease of intensity over the temperature range (Fig.30). The dye did however display a behavior at low temperatures, in the form of a dip followed by a small increase only to start decreasing again. This could be due to the dye behavior or it could also be a feature caused by statistical averaging of the signal peak values.

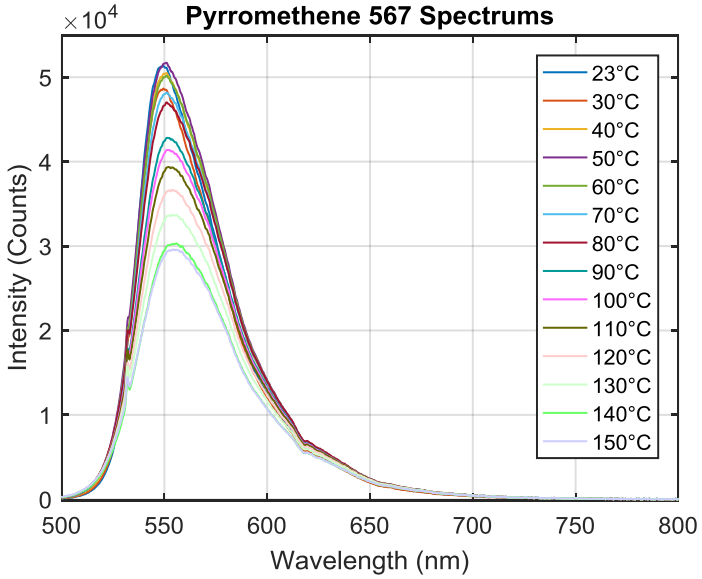

Figure 29: Spectrums of Pyrromethene 567 at different temperatures ranging from room temperature at 23°C up to 150°C.

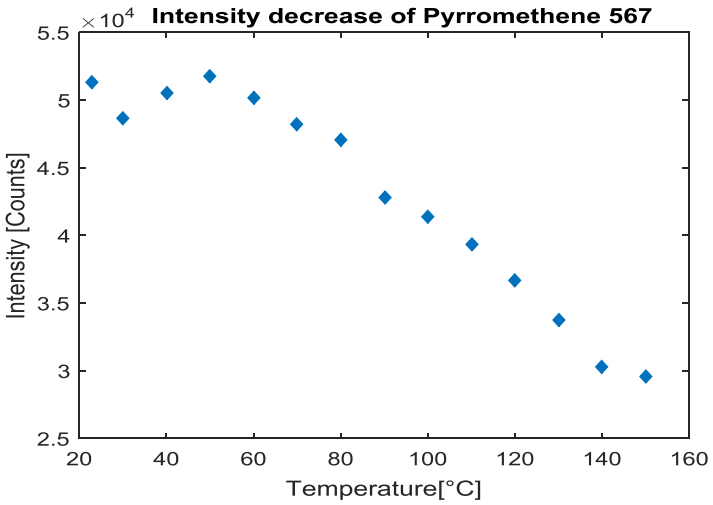

Figure 30: Pyrromethene 567 fluorescence intensity at increasing steps of lubricant oil temperatures.

Pyrromethene 597

The laser energy fluence was averaged around 17.8 J/m^2 with a dye concentration of 0.025 g/L. The intensity of the dye at increasing temperatures can be seen slowly decreasing (Fig. 31 and 32).

All three Pyrromethene dyes proved to have an efficient quantum yield, requiring very low dye concentration for adequate signal. The dye Pyrromethene 597 can be seen to have a large intensity drop over the temperature range tested (Fig.32). For Pyrromethene 567 (Fig.30) one can note a similar drop of intensity but not as drastic. The intensity change due to temperature for Pyrromethene 597 seems to stabilize at higher temperatures which lessens the impact on the fluorescence signal due to temperature fluctuations located at the measuring point. This intensity decrease is expected due to thermal-quenching. Due to the low amount of laser energy used in the evaluation, it should be possible to compensate for the low intensity at higher temperatures by using higher laser energy when preforming real measurements.

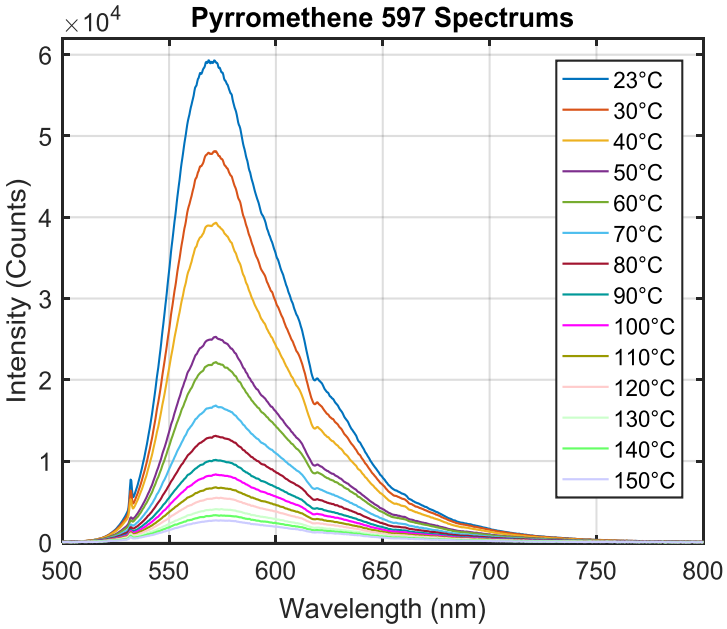

Figure 31: Spectrums of Pyrromethene 597 at different temperatures ranging from room temperature at 23°C up

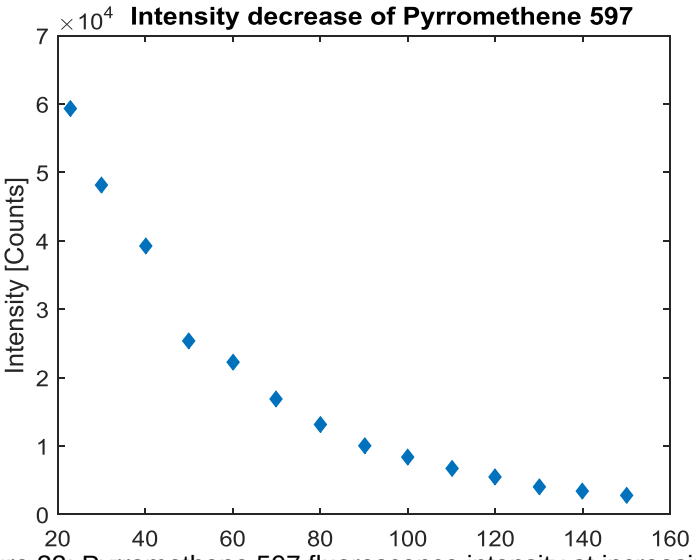

Figure 32: Pyrromethene 597 fluorescence intensity at increasing steps of lubricant oil temperatures.

Both Pyrromethene 597 and Pyrromethene 567 also had their respective fluorescence spectrum overlapping with the lubricants oils own spectrum, making it hard to only measure the dye spectrum. However, both dyes produce significant more fluorescence than the oil, which makes the fluorescence ratio of dye to oil large enough for tracing use. It should also be noted that these two dyes were the easiest to dissolve in the lubricant oil, requiring almost no stirring or heating to be fully mixed.

Pyrromethene 650

The laser energy fluence was averaged around 40.7 J/m^2 with a dye concentration of 0.025 g/L. The intensity of the dye at increasing temperatures can be seen as steadily decreasing (Figure 33 and 34).

Pyrromethene 650 had a constant decrease over the measured temperature range (Fig.34). The fluorescence spectrum was red shifted (Fig.33) compared to the other dyes which allowed for suppression of the oil fluorescence by spectral filtering. This dye had lower quantum efficiency than the other two Pyrromethene dyes and therefore a slightly higher laser energy was required. This dye was used in the 2D-imaging, due to the ability to filter away much of the oil fluorescence spectrum using a bandpass filter. The dye had a crystalized appearance and required more stirring than other dyes to be dissolved in the lubricant oil.

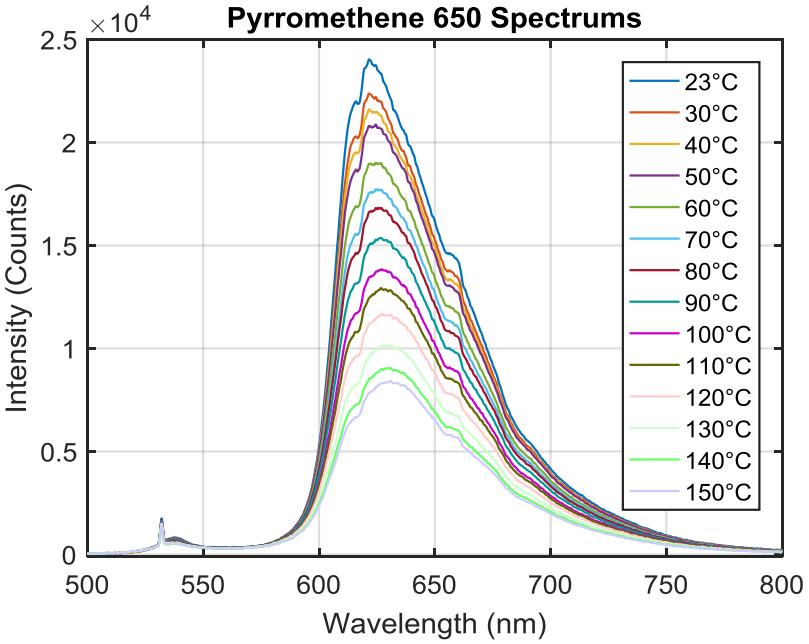

Figure 33: Spectrums of Pyrromethene 650 at different temperatures ranging from room temperature at 23°C up to 150°C.

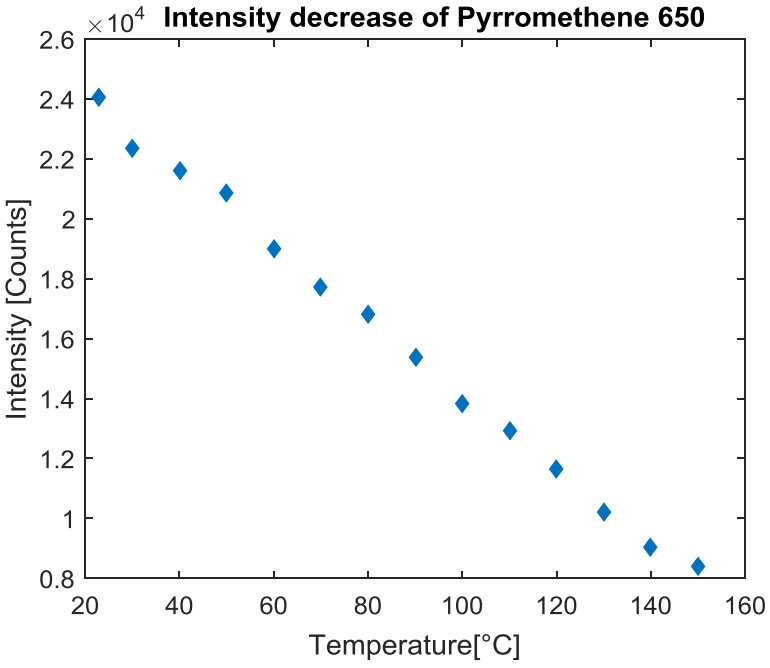

Figure 34: Pyrromethene 650 fluorescence intensity at increasing steps of lubricant oil temperatures

Bestoil Green FYG

This dye was excited using 355 nm. The fluorescence spectrum of the dye was seen between 470 nm up to 600 nm, redshifted approximately 25 nm from the oil spectrum; stretching between 350 nm to 450 nm (Figure 35Figure). The laser fluence was averaged around 45.8 J/m^2 with a dye concentration of 0.25 g/L.

The dye had a low quantum efficiency, requiring around ten times the concentration of the other dyes to achieve satisfactory signal, this makes it realistic to assume a heavier perturbation of the lubricant oil characteristics which is unwanted. The dye spectrum can be seen red shifted enough to enable suppression of the oil fluorescence by spectral filtering (Figure 35). The dye shows a peculiar response to temperature change (Figure 36), it starts off decreasing slowly only to peak at 60°C, later stabilizing at 100°C - 150°C. The behavior is similar to that of Pyrromethene 567 at low temperatures, but much more extreme.

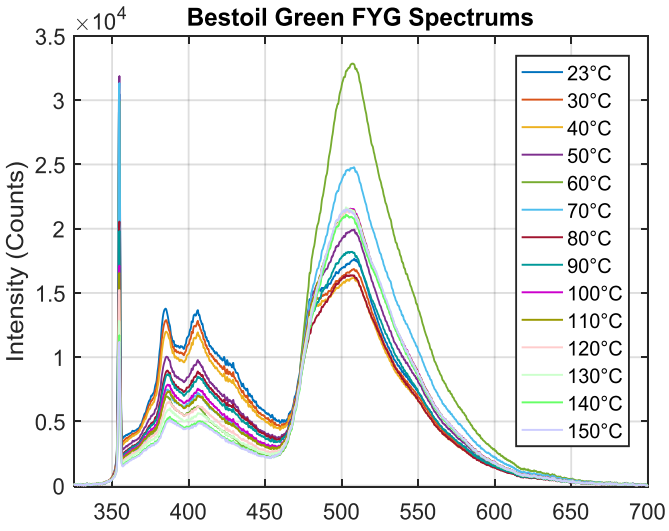

Figure 35: Spectrums of Bestoil Green FYG at different temperatures ranging from room temperature at 23°C up to 150°C.

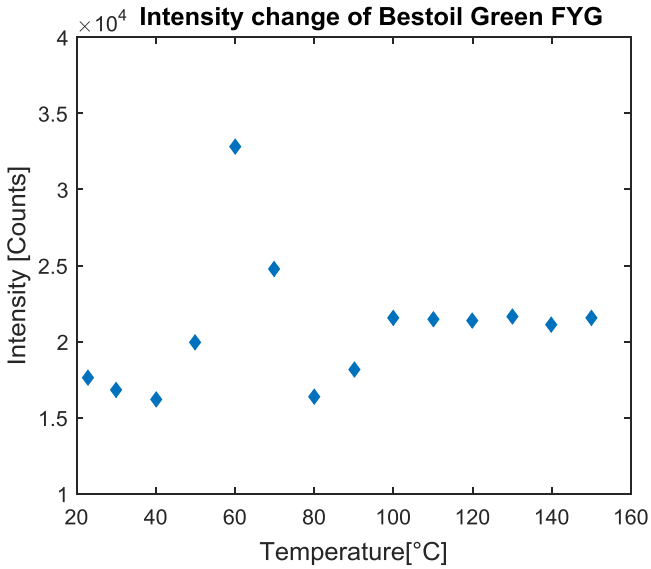

Figure 36: Bestoil Green FYG fluorescence intensity at increasing steps of lubricant oil temperatures.

Rhodamine 590

Rhodamine 590 turned out be not soluble in the lubricant oil used and therefore was not used in further studies. For investigation, the dye was tried in n-heptane but proved to be un-soluble there as well.

Rhodamine 640

Rhodamine 640 seemed to be soluble in the lubricant oil but yielded no signal even when exposed to laser fluence of around 1020 J/m^2. This could be the result of severe quenching or un-solubility in the lubricant oil, therefore this dye was not used for further studies.

DCM

DCM turned out be not soluble in the lubricant oil and therefore was not used for further studies.

2D-Measurement

Pyrromethene 650 was chosen as the tracer for the lubricant oil in this measurement, due to the dyes spectral red shift giving the ability to filter away the fluorescence spectrum of the lubricant oil. This makes easy to distinguish the traced lubricant oil from the non-traced oil.

The result of the Pyrromethene 650 traced lubricant oil by 2D imaging with an ICCD camera show the traced lubricant oil while it is moving across a metal area of 80 cm^2 covered in untraced lubricant oil, while illuminated by the 532 nm laser light. The fluence on the target area was then 1.25 J/m^2. A bandpass filter centered around 589 nm was sued to isolate the dye signal, which gave a signal to noise ratio of 10:1 in the shown figures. Figure 37 and 38 show the oil moving by gravity across the target metal plate.

Figures 39 and 40 show a new traced oil sample, as it moves on the same target plate by pressurized air flow.

The bandpass filter that was used to filter away the oil spectrum limits the fluorescence output of Pyrromethene 650. The filter, centered at 589 nm with a FWHM of 10 nm, transmits only part of the short wavelength side of the dye's fluorescence signal. The goal here is to try to simulate a harsh environment common for in suite measurements in engines, were factors, such as window fouling, will reduce the signal. One can then drastically increase the dye signal by using a filter properly centered at around 624 nm with a FWHM of, for example, 20 nm. The introduced traced oil was later moved around on the target plate using pressured air (Figures 39 and 40). In these figures one can see the untraced lubricant oil in the background, this is possible due to the high pulse energy used and that the filter employed allows transmission of the tail of the oil

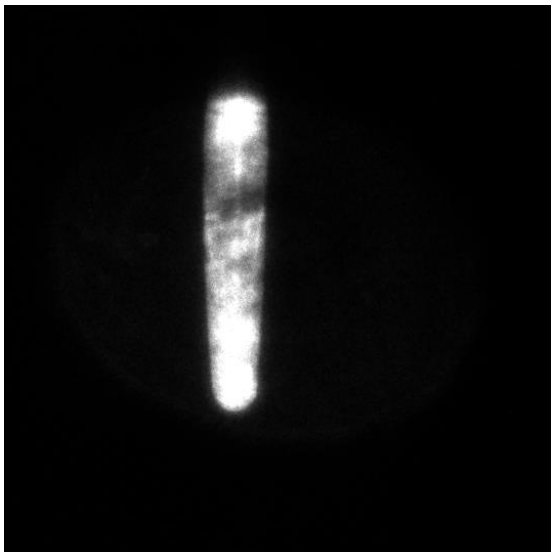

Figure 37: Showing the Pyrromethene 650 traced lubricant oil at a later strage further down the metalplate.

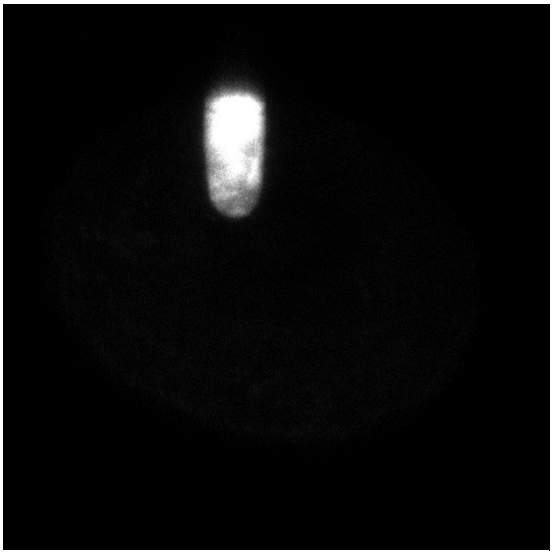

Figure 38: Showing the Pyrromethene 650 traced lubricant oil when introduced to the metal surface covered in un traced oil.

fluorescence spectrum.

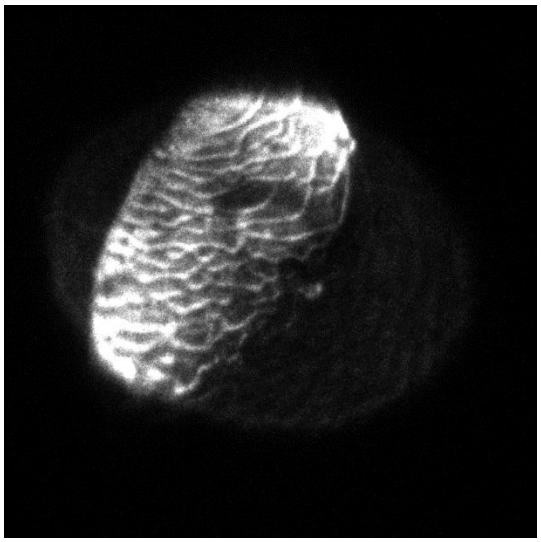

Figure 39: Showing the Pyrromethene 650 traced lubricant oil moved with pressurized air at a later stage, the waves caused by the air can be seen clearly.

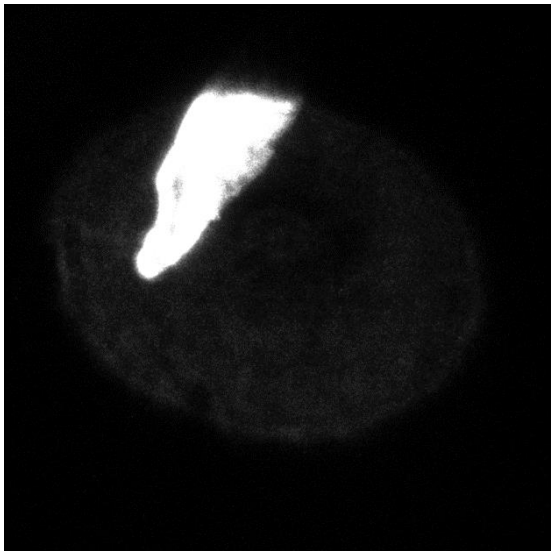

Figure 40: Showing the Pyrromethene 650 traced lubricant oil when introduced to the metal surface, now moved using pressurized air flow.

4 References

[1] Mayer S, Poulsen HH, and Hult J 2010 In-situ optical combustion diagnostics on a large two-stroke marine diesel engine *CIMAC Congress* (Bergen, Norway, June 2010) Paper nbr. 40

[2] Zhang Z 2000 A flexible new technique for camera calibration *IEEE Transactions on Pattern Analysis and Machine Intelligence* **22** 1330–1334

[3] Kurolakos KN and Seitz SM 2000 A theory of shape by space carving *Int. J. of Computer Vision* **38** 199-218